

Boundary-obstructed topological phases

Eslam Khalaf,¹ Wladimir A. Benalcazar,² Taylor L. Hughes,³ and Raquel Queiroz⁴

¹*Department of Physics, Harvard University, Cambridge, MA 02138*

²*Department of Physics, The Pennsylvania State University, University Park, PA 16802, USA*

³*Department of Physics and Institute for Condensed Matter Theory,
University of Illinois at Urbana-Champaign, IL 61801, USA*

⁴*Department of Condensed Matter Physics, Weizmann Institute of Science, Rehovot 7610001, Israel*

(Dated: June 8, 2022)

Symmetry protected topological (SPT) phases are gapped phases of matter that cannot be deformed to a trivial phase without breaking the symmetry or closing the bulk gap. Here, we introduce a new notion of a topological obstruction that is not captured by bulk energy gap closings in periodic boundary conditions. More specifically, we say two bulk Hamiltonians belong to distinct boundary obstructed topological ‘phases’ (BOTPs) if they can be deformed to each other on a system with periodic boundaries, but cannot be deformed to each other for symmetric open boundaries without closing the gap at at least one high symmetry region on the surface. BOTPs are not topological phases of matter in the standard sense since they are adiabatically deformable to each other on a torus but, similar to SPTs, they are associated with boundary signatures in open systems such as surface states or fractional corner or hinge charges. We show that the double-mirror quadrupole model of [Science, 357(6346), 2018] is a prototypical example of such phases, and present a detailed analysis of several aspects of boundary obstructions in this model. In addition, we introduce several three-dimensional models having boundary obstructions, which are characterized either by surface states or fractional corner or hinge charges. We also provide a general framework to study boundary obstructions in free-fermion systems in terms of Wannier band representations (WBR), an extension of the recently-developed band representation formalism to Wannier bands. WBRs capture the notion of topological obstructions in the Wannier bands which can then be used to study topological obstructions in the boundary spectrum by means of the correspondence between the Wannier and boundary spectra. This establishes a form of bulk-boundary correspondence for BOTPs by relating the bulk band representation to the boundary topology.

CONTENTS

	1		24
I. Introduction	1	4. A hinge-obstructed 3D BOTP	24
II. 2D quadrupole insulator and boundary obstructions	3	C. 3D BOTPs with anomalous surface states	24
A. Review of the quadrupole insulator model	3	1. Dimerized weak Chern insulator	25
B. Real space picture	4	2. Dimerized weak quantum spin Hall insulator	25
C. Wannier bands and edge spectrum	6	V. Discussion	26
D. Corner charge and filling anomalies	8	Acknowledgments	27
1. Filling Anomaly	8	A. Character table of D_2^π	28
2. Real space understanding of filling anomalies	9	B. Real Space Proof of Anti-commuting Symmetries	28
3. Filling anomalies for edge vs bulk obstructions	10	1. Anticommuting Mirrors in the 2D DMQI	28
III. Boundary obstructions: Generalities	11	2. Anticommuting C_2 and M_z for 3D C_{2nh} Models	28
A. General definition	11	C. Band representations and movable Wyckoff positions	28
1. Relationship to HOTIs	12	D. Bulk band representation of the DMQI model	29
2. Diagnosing BOTPs using Wannier spectrum	13	References	30
B. Band representations of BOTPs	14		
1. Wannier band representations	14		
C. Boundary signatures	15		
1. BOTPs with surface states	15		
2. BOTPs with filling anomalies	16		
D. Other 2D models	16		
IV. 3D models with boundary obstructions	18		
A. Recipe for constructing 3D BOTPs	18		
B. 3D BOTPs with filling anomalies	19		
1. A new class of C_{2nh} Hamiltonians	19		
2. Real space picture and filling anomaly	20		
3. Wannier spectrum	22		

I. INTRODUCTION

A symmetry protected topological (SPT) phase is a gapped phase of matter that cannot be adiabatically deformed to a trivial phase without breaking the symmetry or closing the bulk energy gap [1–8]. For free fermion systems with internal symmetries, a complete understanding of SPTs was achieved in

the pioneering work of Refs. [4, 9–11]. In any given symmetry class and dimension (d), an SPT hosts anomalous gapless ($d-1$)-dimensional surface states whose existence is tied to the non-trivial bulk topology. This connection between bulk and boundary topological properties is known as a bulk-boundary correspondence.

For spatial or crystalline symmetries, the relationship between bulk and boundary topological signatures can be more subtle. On one hand, there are topological crystalline phases, such as mirror Chern insulators [12, 13], that exhibit a conventional bulk-boundary correspondence signaled by the appearance of 2D gapless surface states on any mirror invariant surface plane. On the other hand, less traditional types of surface states, known as higher-order surface states [14–24], which have a lower dimensionality, e.g., states confined to corners or hinges of the sample, are also possible in systems with crystalline symmetry. Even in the absence of any mid-gap surface (or higher-order boundary) states, additional signatures such as fractional charge at corners [25] or defects [14, 26–28] can be used to distinguish different SPTs. Furthermore, there are some bulk SPTs protected by crystalline symmetries that are not associated with surface states or boundary fractional charges at all. For instance, two atomic insulators corresponding to filling the same Wyckoff positions, but with orbitals that transform *differently* under site symmetries, cannot be smoothly deformed to each other, but they cannot be distinguished by surface states or corner charges either. Thus, for SPTs protected by crystalline symmetries, bulk topological distinctions do not always imply boundary signatures in the form of gapless states or fractional charges at the boundary.

The purpose of this work is to investigate the reverse question. Rather than asking whether the distinction between two bulk SPTs can be captured by a boundary signature, we ask whether two systems which exhibit different boundary signatures, e.g., low-energy modes or fractional charges, necessarily correspond to topologically distinct systems in the bulk. There is an obvious counter-example to this statement corresponding to the case where non-trivial SPTs are placed on the boundary of a trivial bulk. For example, one can imagine gluing 2D layers on the surface of a 3D trivial insulator. If these layers are gapless in their two-dimensional bulk, then the 3D system will have surface states. If the layers are 2D topological insulators instead, then the system will exhibit gapless hinge modes. However, these boundary signatures are not associated with a bulk property. Some of these phases fall under the category of “extrinsic higher-order” phases which are sensitive to surface terminations [22, 24]. However, after excluding these cases, it is unclear if it is possible to find topologically protected boundary modes that can be created or destroyed simply by tuning parameters of the bulk Hamiltonian, but *without* closing the bulk gap.

One of the first examples of this phenomenon is provided by the quadrupole model of Ref. 15. This is a 2D model with gapped bulk and edges that hosts quantized fractional charge at the corners. Two symmetry variants of the model were considered: one with fourfold rotation symmetry C_4 which satisfies $C_4^4 = -1$, and the other with two anticommuting mir-

ror symmetries. In the former case, the quadrupole phase is a topological phase in the standard sense: it is an obstructed atomic limit [29] separated from the trivial atomic limit by a bulk gap-closing phase transition. However, in the latter case, the quadrupole phase is not a topological phase in the standard sense since the value of the quadrupole moment can be changed without closing the bulk gap (in periodic boundary conditions). The topology in this model is captured by a more subtle distinction contained in the spectrum of the Wilson loop operators (Wannier spectrum), or in the entanglement spectrum, rather than the bulk energy spectrum. This was argued to imply that the two phases of the model are separated by an edge (rather than a bulk) phase transition when considered with open boundary conditions [15, 16]. Indeed, since both the gaps in the bulk and on the edge protect the quantized corner charge, one can imagine the corner charge delocalizing along the edges and changing values if the edge gap closes.

Despite the number of subsequent works that have studied several aspects of the quadrupole model and its generalizations, the subtle topological distinction captured by the double-mirror quadrupole insulator (DMQI) has ramifications that have been mostly overlooked. In particular, several questions regarding the nature of topological distinctions that are not captured by a bulk phase transition remain unanswered. These include: (i) how can one, in general, define a topological distinction that does not involve a gap closing phase transition in the bulk? (ii) are there other examples of models in two or three dimensions that exhibit similar phenomenology? (iii) under what conditions does an obstruction in connecting two Wannier spectra indicate a gap-closing transition at the boundary?, and (iv) how is this related to boundary signatures, e.g., fractional corner charge, or boundary states, in a general setting?

In this work, we answer these questions by introducing the concept of boundary obstructed topological phases (BOTPs) that captures distinctions between Hamiltonians that can be adiabatically connected with periodic boundary conditions, but cannot be connected for symmetric surface terminations with open boundary conditions. We provide a general definition of such distinctions, and show how they can be understood in terms of the Wannier spectra as well as real-space symmetry representations.

In order to make the presentation as clear as possible, we will first start with detailed explanations of different aspects of the boundary obstruction concept that are realized in the DMQI. Then we will move on to discuss the general aspects of boundary obstructions. After reviewing the DMQI model in Sec. II A, we provide a real space framework for its boundary obstruction in Sec. II B, followed by a detailed analysis of the Wannier spectra, and how they relate to the physical edge spectra of particular surface terminations, in Sec. II C. Afterwards, we establish how the boundary obstruction in the DMQI model is related to the existence of fractional corner charge via a detailed symmetry analysis of the model with open boundaries in Sec. II D.

After the detailed study of the DMQI model, we introduce the general definition of boundary obstructed phases, and discuss their stability in Sec. III A. In Sec. III B we show how to

diagnose boundary obstructions through real-space band representations of the Wannier bands themselves, before showing how the definition can be related to boundary signatures such as surface states or fractional charges in Sec. III C. Afterwards, we discuss other possible 2D models with boundary obstructions in Sec. III D and show that, apart from the DMQI (and variants of it), all such models require specific, complicated surface terminations to probe the boundary obstructions and the associated corner charges. In Sec. IV we introduce a general recipe to generate 3D models with various types of boundary obstructions from a 2D building block. Such obstructions can be associated with fractional corner charges, fractional hinge charge density (Sec. IV B), or surface states (Sec. IV C) depending on the choice of the 2D building block. For example, in the latter case we introduce two 3D models built from either a 2D Chern insulator or a 2D quantum spin Hall insulator with robust one dimensional states localized at their hinges. We also provide a complete characterization of all the 3D models using the Wannier spectra. Finally, we close with some concluding remarks and discussion in Sec. V.

II. 2D QUADRUPOLE INSULATOR AND BOUNDARY OBSTRUCTIONS

A. Review of the quadrupole insulator model

We start our discussion by reviewing the DMQI model introduced in Ref. [15]. It consists of four orbitals describing spinless fermions arranged on a two-dimensional rectangular lattice with dimerized hopping amplitudes along the x and y directions, and π -fluxes threaded through each plaquette as shown in Fig. 1. The Bloch Hamiltonian is given by

$$\mathcal{H}(\mathbf{k}) = [\gamma_x + \lambda_x \cos(k_x)] \Gamma_4 + \lambda_x \sin(k_x) \Gamma_3 + [\gamma_y + \lambda_y \cos(k_y)] \Gamma_2 + \lambda_y \sin(k_y) \Gamma_1, \quad (1)$$

where γ_x and γ_y are hopping amplitudes within a unit cell along x and y respectively, and λ_x and λ_y are the inter-cell hopping amplitudes to nearest neighbor unit cells. The negative signs, represented by the dashed lines in Fig. 1a, are a gauge choice for the π -flux threaded through each plaquette. The $\Gamma_{0,\dots,4}$ matrices satisfy $\{\Gamma_i, \Gamma_j\} = 2\delta_{i,j}$, and are represented explicitly by $\Gamma_0 = \sigma_3\tau_0$, $\Gamma_k = -\sigma_2\tau_k$, $\Gamma_4 = \sigma_1\tau_0$ for $k = 1, 2, 3$, where $\sigma_{0,\dots,3}$ ($\tau_{0,\dots,3}$) denote the Pauli matrices, and the tensor product is implicit.

The model in Eq. 1 has reflection symmetries along both x and y , which for spinless electrons satisfy $M_x^2 = M_y^2 = 1$. They are represented by

$$M_x \mathcal{H}(k_x, k_y) M_x^\dagger = \mathcal{H}(-k_x, k_y), \quad M_x = \sigma_1 \tau_3, \\ M_y \mathcal{H}(k_x, k_y) M_y^\dagger = \mathcal{H}(k_x, -k_y), \quad M_y = \sigma_1 \tau_1. \quad (2)$$

The model is also invariant under the combination $M_x M_y = C_2$, where C_2 is a two-fold rotation symmetry. The π -flux leads to the anticommutation of the two reflection operators $\{M_x, M_y\} = 0$. As a result, C_2 satisfies $C_2^2 = -1$, as would be the case for spinful fermions. Other than the crystalline

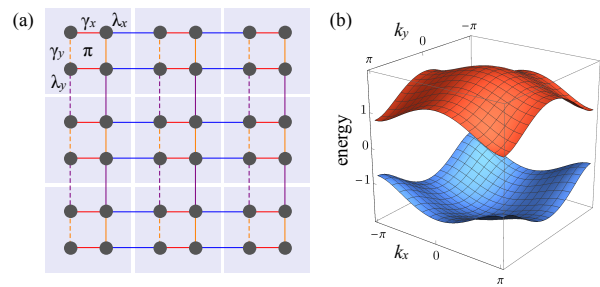


FIG. 1. Lattice model used to define the quadrupole insulator in Eq. 1. In (a), dashed lines have a relative negative sign to account for a flux of π threading each plaquette. The flux is the origin of the anticommuting reflection operations. (b) Band structure of the quadrupole insulator with $\gamma_x/\lambda_x = 0.5$ and $\gamma_y/\lambda_y = 0.4$. Each energy band is twofold degenerate for a total of four bands.

symmetries, the model $\mathcal{H}(\mathbf{k})$, as written, lies in class BDI, i.e., it has time-reversal, chiral, and charge conjugation symmetries.

The point group G of $\mathcal{H}(\mathbf{k})$ in (1), which we denote D_2^π , is isomorphic to the dihedral group D_4 . The full group structure is obtained by adding the element $\bar{1} = (M_x M_y)^2$ to the spinless point group D_2 to accommodate the anticommutation of the two reflections, with $M_x^2 = M_y^2 = \bar{1}^2 = 1$. The dihedral group D_2^π has four one-dimensional, irreducible representations (A_1, A_2, B_1, B_2), and one two-dimensional irreducible representation (\bar{E}) odd under $\bar{1}$ (see Appendix A). In the present realization, $\bar{1}$ acts locally both in real and momentum space.

The energy spectrum of the Hamiltonian (1) is two-fold degenerate and gapped across the entire bulk Brillouin zone (BZ) (cf. Fig. 1) unless both $|\gamma_x/\lambda_x| = 1$ and $|\gamma_y/\lambda_y| = 1$. Hence, we can connect the Hamiltonians at any pair of points in the $(\gamma_x/\lambda_x, \gamma_y/\lambda_y)$ -plane without closing the bulk gap. This implies the absence of any bulk topological distinctions in the model. We note that the presence of C_4 symmetry alters this conclusion since it forces $\lambda_x = \lambda_y = \lambda$ and $\gamma_x = \gamma_y = \gamma$, thus changing the sign of $|\gamma/\lambda| - 1$ is necessarily accompanied by a bulk-gap-closing phase transition, which indicates that the model has at least two distinct bulk-protected topological phases.

Despite the absence of bulk topological distinctions in the model protected by mirror symmetries, Refs. 15 and 16 have uncovered a more subtle topological distinction encoded in the topology of the Wannier bands instead. The Wannier bands along the $x(y)$ direction are obtained by taking the Wilson loop along this direction for a fixed momentum $k_y(k_x)$ [30, 31]. The Wilson loop operator $\mathcal{W}^i(\mathbf{k})$, $i = x, y$ is a unitary operator whose eigenvalues have the form $e^{2\pi i \nu_i(\mathbf{k}_{i\perp})}$. The values $\nu_i(\mathbf{k}_{i\perp})$ are defined modulo one and determine the positions (within the unit cell) of the charge center for the hybrid Wannier states which are maximally localized in the i -direction, but are delocalized Bloch waves with momentum $\mathbf{k}_{i\perp}$ in the perpendicular direction(s) [30, 31]. For the DMQI model, the two Wannier bands of the occupied states are generally gapped and symmetrically displaced away from

the high-symmetry lines $\nu_i = 0$ and $\nu_i = 1/2$ (cf. Fig. 2b). Among other things, this indicates that there is no spectral flow as would be the case, for example, for a strong topological insulator [32].

Whenever the two Wannier bands are separated by gaps from above and below we can consider the projector onto one of these two bands. This projector is effectively projecting onto the ground state of a 1D reflection-symmetric insulator with one electron per unit cell. Such an insulator can be characterized by a half-quantized polarization p distinguishing the cases where the charge center is at the center ($p = 0$), or the edge ($p = 1/2$), of the 1D unit cell. Since there are two possible sets of Wannier spectra, i.e., one along the x -direction and one along the y -direction, there are two distinct quantized Wannier band polarizations $p_{x,y} = 0, 1/2$ and $p_{y,x} = 0, 1/2$ where $p_{i,j}$ denotes the polarization in the j -direction for a band taken from the Wilson loop in the i -direction. This yields a $\mathbb{Z}_2 \times \mathbb{Z}_2$ invariant capturing the topology of the Wannier bands. Such invariants are protected by the gap in the Wannier spectrum rather than the energy spectrum, which means that their value can be changed without going through a bulk gap closing. As we will explain in detail later, these types of transitions can *in some cases* be associated with an energy gap-closing at the *edge*, rather than the bulk, when the system is considered with open boundary conditions in both directions. This will be the topic of Sec. II C.

For $\mathbf{p}^\nu = (p_{x,y}, p_{y,x}) = (1/2, 1/2)$, the model exhibits zero-energy corner modes when considered on a rectangular geometry with open boundaries in both directions. However, these corner modes are protected by particle-hole symmetry which can be broken without changing the Wannier band polarization (whose quantization relies only on mirror symmetries). Thus, these corner modes are not associated with the quantized Wannier band polarization. Instead, as we will show in Sec. II D, we can associate the $(1/2, 1/2)$ phase with corner *charge* [15, 16, 25, 27].¹

Following this review of the DMQI, we will dedicate the remainder of this section to show that the topology of the DMQI can be captured using the notion of edge topological obstructions; a new type of topological obstruction that is only present when the model is placed on certain geometries with open boundary conditions. In particular, we will provide an intuitive picture for a topological obstruction that is associated with an edge gap-closing transition rather than a bulk one. Furthermore, we will show how the $\mathbb{Z}_2 \times \mathbb{Z}_2$ topological distinction encoded in the Wannier band polarizations is related to the corner charge, which is determined by only a single \mathbb{Z}_2 invariant that distinguishes $\mathbf{p}^\nu = (1/2, 1/2)$ from the other three cases. We note here that picking $\mathbf{p}^\nu = (1/2, 1/2)$ as the non-trivial phase relies on the standard boundary termination consistent with the unit cell chosen in defining the Hamiltonian (1). As we will discuss later, the choice of the boundary

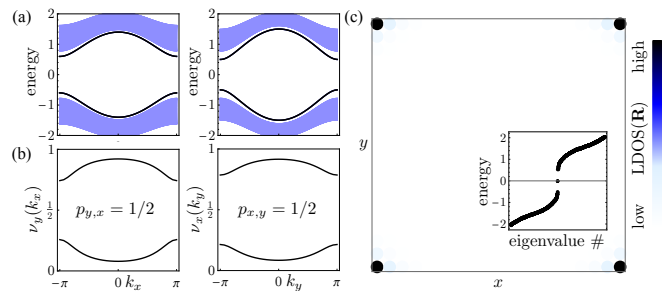


FIG. 2. (Color online) (a) Band structure of the two-dimensional quadrupole insulator with open boundaries in a single direction, y (left) or x (right). The blue bands correspond to the bulk band continuum, and the black bands that are slightly separated from the bulk bands are localized at the edges. (b) Wannier bands $\nu_y(k_x)$ (left) and $\nu_x(k_y)$ (right), with a quantized Wannier band polarization of $p_{x,y} = p_{y,x} = 1/2$. The Wannier spectra are topologically equivalent to the surface bands in (a) when we identify the gap around $\nu_i(k) = 1/2$ to represent the surface gap, see Sec. II C. (c) Local density of states at zero energy $\text{LDOS}(\mathbf{r}) = -\pi^{-1} \text{Im tr}(H(\mathbf{r}) + i\eta)^{-1}$ for a small broadening $\eta = 0.1$ in a system with open boundaries in x and y . The inset shows the existence of zero energy states inside the gap.

decides which Wannier phase is distinguished from the others. In all cases, however, the resulting classification for a fixed boundary is \mathbb{Z}_2 .

B. Real space picture

In the following, we will present an understanding of the edge topological obstruction of the DMQI in terms of a real space picture. At half-filling, the space of filled bands is Wannier representable, i.e., it is possible to find a basis of localized symmetric orbitals that span the subspace of filled bands. In a Wannier representable system, localized orbitals are labelled by their so-called Wyckoff position $\mathcal{Q} = \{q_\alpha\}$ which denotes a *set* (symmetry orbit) of spatial positions q_α with $\alpha = 1, \dots, N_{\mathcal{Q}}$ which is invariant as a whole under the symmetry group G . The positions q_α can map to each other under some elements of G , but they are invariant under a (site symmetry) subgroup $G_q \subseteq G$ ². $N_{\mathcal{Q}}$ denotes the size of the set of spatial positions q_α , and is called the Wyckoff multiplicity of position \mathcal{Q} . Wannier representable (atomic) insulators have electronic configurations constructed by decorating the various Wyckoff positions with orbitals that transform under site-symmetry representations of G_q . These different Wannier representable phases are each associated with a *band representation* (BR) [29, 33–35] that encodes both its transformations under the symmetry group, and its momentum-space Zak-Berry phases. A short introduction to BRs and their derivation from the G_q representations can be found in App. C.

¹ It is worth noting that the fractional corner charge can be removed by adding edge degrees of freedom. Adding fractional corner charge to the trivial phase, will interchange which phase we identify as topologically non-trivial, but the fact that the two phases can be distinguished by the fractional corner charge remains true.

² The site symmetry groups for different elements q_α in the same Wyckoff position are equivalent up to conjugation, so we denote them by the same symbol G_q .

In the DMQI case, the model is defined on a lattice with two perpendicular, and anticommuting, mirror symmetries M_x and M_y (point group D_2^{π}). This point group has the same set of Wyckoff positions as the point group D_2 : (i) four maximal Wyckoff positions with multiplicity 1 corresponding to positions lying at the intersection of the two mirror-invariant lines, i.e., at positions $(0, 0)$, $(0, 1/2)$, $(1/2, 0)$ and $(1/2, 1/2)$ (labelled $1a$, $1b$, $1c$ and $1d$, respectively), (ii) four Wyckoff positions with multiplicity 2 corresponding to positions lying along one of the mirror-invariant lines, $(\pm x, 0)$, $(\pm x, 1/2)$, $(0, \pm y)$, $(1/2, \pm y)$, (labelled $2e$, $2f$, $2g$, and $2h$, respectively), and (iii) one general Wyckoff position $4i$ with multiplicity 4 at four generic symmetry-related points $(\pm x, \pm y)$.

To illustrate the absence of a bulk obstruction in the DMQI model, consider a translationally invariant lattice with M_x and M_y symmetries having periodic boundary conditions³. For a filling of two electrons per unit cell, there are only three allowed options for placing the atomic orbitals: (i) both are placed at the *same* maximal Wyckoff position, (ii) the two orbitals are placed at *different* maximal Wyckoff positions, or (iii) they are placed at a Wyckoff position of multiplicity two. Case (ii) has a non-vanishing polarization of $1/2$ along x or y (or both) which rules it out for the DMQI model for which both polarizations vanish. Interestingly, cases (i) and (iii) may be adiabatically deformed into each other in some cases, i.e., they may belong to *equivalent* band representations. This is the situation when the two electrons (per cell) are in the two dimensional representation of the D_2^{π} point group, i.e., when the matrix representations of the two mirror operators anticommute when acting on the electron orbitals. To show this, we note that equivalence between two band representations can be demonstrated if there is a symmetric, adiabatic deformation between the two configurations[29, 36]. In Appendix B we show that in order to carry out such a continuous deformation between Wyckoff position configurations, the two mirror operators are required to anticommute, which is exactly the case for the DMQI model. The necessity for anticommutation of mirror operators was previously proven in Ref. [15, 16] using the symmetry indicators of the Wannier bands, where it was shown to be linked to the existence of gaps in the Wannier spectra.

In Fig. 3 we show how to deform the configuration with both centers at $1a$ to the one where both are at $1d$ while preserving the symmetry and the bulk gap. This is done by first moving the two orbitals horizontally along the $y = 0$ line (via the Wyckoff position $2e$) to $1c$, then moving them vertically along the $x = 1/2$ line (via the Wyckoff position $2h$) to $1d$. It is instructive again to compare to the model with C_4 symmetry for which there is no Wyckoff position with multiplicity two. In this case, it is impossible to move two electrons from $1a$ to $1d$ without breaking the symmetry, indicating that the

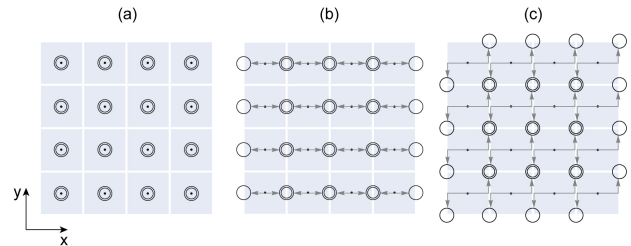


FIG. 3. Deformation of the Wannier centers (open circles), in the double-mirror quadrupole model, from the $1a$ to the $1d$ Wyckoff position along movable Wyckoff positions. We see that from panel (b) to panel (c) we cannot preserve the symmetry at the edges.

two correspond to distinct bulk phases.

Now we are ready to illustrate the real-space picture of boundary obstructions. We will show that the process which allows the deformation between configurations $1a$ and $1d$, while possible in a system with periodic boundary conditions, is impossible (without breaking the mirror symmetries) in a system with a rectangular geometry with open boundary conditions in the x and y directions, as shown in Fig. 3. To see this, we note that there are two possible ways to symmetrically move two electrons from $1a$ to $1d$. The first one goes through $1c$ by first moving horizontally through $2e$ then vertically through $2h$, whereas the second goes through $1b$ by first moving vertically through $2g$ then horizontally through $2f$. We note, however, that in the presence of the vertical boundary at $x = 1/2$, the electron filling of position $1c$ on the edge is half of its filling in the bulk (since such a site is shared by two unit cells when in the bulk, but one of them is now absent on an edge). This means that there is only one electron at the $1c$ position at the edge, instead of two, which makes it impossible to vertically move it to position $1d$ while preserving the symmetry and energy gap. Similarly, the presence of the horizontal edge at $y = 1/2$ prohibits the deformation $1a \rightarrow 1b \rightarrow 1d$ as position $2f$ is unavailable at the edge. Thus, with open boundaries we can pass from $1a$ to $1b$ or $1c$, but not $1d$, which distinguishes $1d$ from the other three configurations in the presence of open boundaries.

To summarize, there are two ways to move two electrons from $1a$ and $1d$: one of which goes through position $1c$ and one through $1b$. Importantly, each of the two edges (x or y) prohibits only *one* of the two trajectories. Thus, if we open the boundaries along only one direction by considering the system on a cylinder, it is still possible to deform $1a$ to $1d$, and thus they are not distinguished. However, once we take open boundaries along both the x and y directions (with an edge the termination consistent with the unit cell), these two atomic configurations cannot be continuously connected while preserving the symmetry. Thus, the DMQI exhibits what we will call an *edge obstruction* wherein two phases can be smoothly deformed to each other in the bulk, but there exists an edge termination such that any such smooth, symmetry preserving deformation involves an edge gap closing.

³ In general, point group operations act non-locally in real-space, and generically relate orbitals in different unit cells. However, one can use translation symmetry on a transformed orbital to shift it back to the initial unit cell. This allows us to represent the different point-group operations as an action on Wannier centers inside a unit cell.

C. Wannier bands and edge spectrum

We now switch our attention to the diagnosis of the edge obstruction in terms of the Wannier spectrum. As discussed in Sec. II A, and Refs. 15 and 16, the Wannier bands of the DMQI model can be characterized by a $\mathbb{Z}_2 \times \mathbb{Z}_2$ invariant $\mathbf{p}^\nu = \frac{1}{2}(\Theta(1 - |\gamma_x/\lambda_x|), \Theta(1 - |\gamma_y/\lambda_y|))$ (where $\Theta(x)$ is the step function). Using the correspondence between the Wannier spectrum and the edge spectrum [37], we may naively think that the DMQI has four distinct phases that cannot be smoothly connected to each other without closing the energy gap at the edge. This, however, contradicts the analysis of the previous sections where we only found two, rather than four, distinct phases due to the edge obstruction.

The resolution to this puzzle lies in the observation that the edge spectrum and the Wannier spectrum differ in one fundamental aspect, despite being smoothly deformable to each other. Namely, the Wannier spectrum is periodic, whereas the edge spectrum is not. This means that of the two gaps of the Wannier spectrum, one at $\nu = 0$ and one at $\nu = 1/2$, only one corresponds to the actual energy gap at the edge. Thus, only Wannier transitions which involve closing this particular gap correspond to actual edge obstructions. The determination of which Wannier gap corresponds to the edge energy gap depends on details, including the surface termination as we will see below.

To understand the relationship between a surface spectrum and a Wannier spectrum, let us follow Ref. 37 in implementing the edge via the replacement $\mathcal{H} \rightarrow \tilde{\mathcal{H}}(x) = P\phi_M(x)P + M(1-P)$ where P is the projector onto the filled bands of the original Hamiltonian \mathcal{H} , and $\phi_M(x)$ is the regularized linear potential given by

$$\phi_M(x) = \begin{cases} x, & |x| < M \\ \text{sgn}(x)M, & |x| > M. \end{cases} \quad (3)$$

For a given filling specified by a chemical potential μ satisfying $-M < \mu < M$, this Hamiltonian reduces to the spectrally-flattened bulk Hamiltonian with filled (empty) states at energy $-M$ (M) in the bulk. Thus, $\tilde{\mathcal{H}}(x)$ has the same filled states as \mathcal{H} deep within the sample, and it implements the vacuum Hamiltonian, where all eigenstates are empty (trivial projection operator), far outside the sample. The linear potential is special since it sets a direct proportionality between distance and energy⁴.

The resulting spectrum of \tilde{H} is shown in Fig. 4. We can see that the spectrum for the states localized close to the edge consists of several copies of the Wannier spectrum shifted relative to each other by some integer. The rest of the spectrum far away from the edge accumulates close to energies $\pm M$ which indicate states in the bulk ($\pm M$) or outside of the

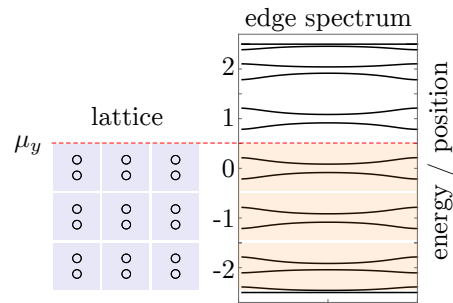


FIG. 4. Spectrum for the Hamiltonian $\tilde{\mathcal{H}}(x)$ implementing the edge termination with the linear potential $\phi_M(x)$ (Eq. 3) truncated at $M = 2.5$. We can see that the spectrum for energies localized close to the edge matches exactly the Wannier spectrum. Bulk states are all accumulated at energies $\pm M$.

sample ($+M$). It is clear from Fig. 4 that, in this potential, the edge termination is decided by choosing an energy that separates the filled states inside the sample from the empty states outside, i.e., an “edge chemical potential.” The linear form of the potential gives a direct relation between the edge chemical potential and the “position” of the edge termination. Since the edge energy spectrum is just repeated copies of the Wannier spectrum, the edge chemical potential determines a corresponding “Wannier chemical potential” (WCP). The key implication of this analysis is that Wannier gap-closings that happen only at a position corresponding to the WCP indicate a gap closing in the edge energy spectrum. *This establishes the important link between gap closings in the Wannier spectrum and at the edge.*

In the following, we will set a convention to simplify our analysis. We always choose the unit cell to be centered at $(0,0)$ so that its edges lie on the lines $x = 1/2$ and $y = 1/2$ (in 2D), and we restrict ourselves to lattice terminations respecting the unit cell. This means that the edge termination at $x = 1/2$ ($y = 1/2$) corresponds to the WCP $\nu_x = 1/2$ ($\nu_y = 1/2$). Consequently, a Wannier gap-closing at $\nu_x = 1/2$ or $\nu_y = 1/2$ represents a genuine edge gap closing in our convention, whereas a gap-closing at $\nu_x = 0$ or $\nu_y = 0$, does not. Instead the latter type of gap closing indicates mixing between different states at the edge, or states at the edge mixing with the bulk, without closing the edge gap.

Using the preceding analysis, we can now show that the state having $\mathbf{p}^\nu = (1/2, 1/2)$ is distinct from the other three Wannier polarization configurations (for our choice of lattice termination). The latter three can all be continuously connected while preserving symmetry, but there is an edge obstruction when trying to go from one of $(0,0)$, $(1/2,0)$, $(0,1/2)$ to $(1/2,1/2)$. We can use Fig. 5 to illustrate this conclusion. This figure provides a diagram of all possible Wannier band phases as a function of the ratios γ_x/λ_x and γ_y/λ_y . The blue central square in the diagram corresponds to the Wannier polarization $\mathbf{p}^\nu = (1/2, 1/2)$; whereas other regions correspond to Wannier polarization equal to either $\mathbf{p}^\nu = (1/2, 0)$ (orange regions), $\mathbf{p}^\nu = (0, 1/2)$ (red regions), or $\mathbf{p}^\nu = (0, 0)$ (white regions). As we can see from the figure, going from

⁴ To match the units between energy and distance, we note that the Hamiltonian $\tilde{H}(x)$ is a dimensionless band-flattened Hamiltonian where filled (empty) bands correspond to $-M$ ($+M$). Similarly, the position x is measured in units of the lattice constant and can be taken to be dimensionless.

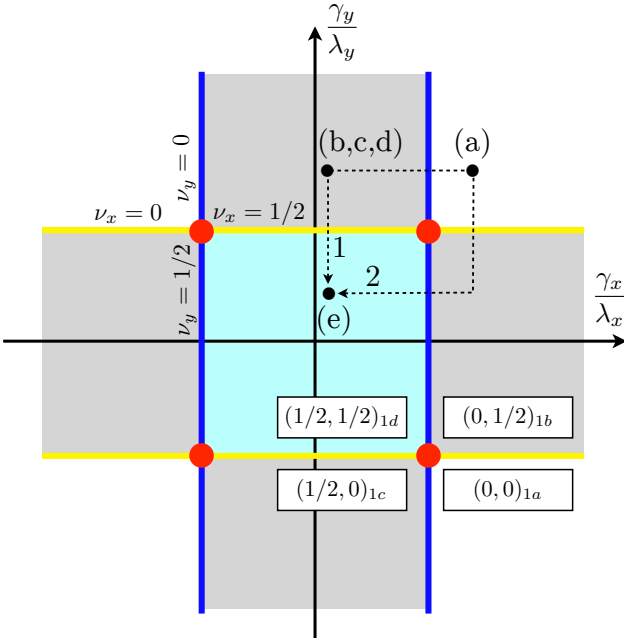


FIG. 5. Diagram of the phases of the Wannier bands of the DMQI model, Eq. 1. On the yellow and blue lines a Wannier gap-closing transition occurs in the Wannier spectra \mathcal{W}^x and \mathcal{W}^y , respectively. The gap closing occurs either at $\nu_i = 0$ or $\nu_i = 1/2$ as indicated. At the intersection of the two lines, marked with a red dot, the bulk spectrum is gapless. To each region, we can associate the nested polarization $\mathbf{p}_{\mathcal{Q}}^{\nu}$, where \mathcal{Q} indicates the maximal Wyckoff position associated to \mathbf{p}^{ν} . Black dots indicate specific configurations corresponding to the plots (a-e) in Fig. 6 where we show the evolution of \mathcal{W}^x and \mathcal{W}^y along the path 1, indicated with a dashed line. The phase 1d is always separated from the remaining ones by a Wannier gap closing at the Wannier chemical potential $(\mu_x, \mu_y) = (1/2, 1/2)$, and hence is separated by a gap closing at the physical boundary for our choice of boundary termination. Choosing a different path from (a) to (e), for example dashed line 2, would still imply a boundary gap closing although at a different edge.

the $(1/2, 1/2)$ phase to any other phase involves *at least one* Wannier transition at $\nu_x = 1/2$ or $\nu_y = 1/2$, whereas going between any of the three other phases can be achieved without a Wannier transition at $\nu_i = 1/2$. We can conclude that, in our convention, the $(1/2, 1/2)$ phase is separated from the other three phases by an edge gap-closing, whereas the three other phases are continuously connected, i.e., any pair of them can be smoothly connected without closing the edge gap or breaking symmetry. This is the resolution to the discrepancy between the topological characterization in terms of edge spectrum vs. Wannier spectrum. We note that if we changed our edge termination, e.g., choosing to terminate the unit cell at $x = 0, y = 1/2$, the only effect would be to permute which of the four polarization configurations should be distinguished from the other three.

Having set up this background, we can now study the connection between Wannier polarization and the real space picture of the edge obstruction. Fig. 6 shows a detailed version of the deformation process in Fig. 3, and illustrates the different Wannier polarization configurations associated with each

intermediate state. In Fig. 6(a), we have a phase characterized by $\mathbf{p}^{\nu} = (0, 0)$. As the Wannier centers are separated horizontally away from $1a$, a first Wannier transition occurs between Fig. 6(a) and (b) where the y -Wannier gap closes at $\nu_y(k_x = \pi) = 0$. If we interpret the edges of the geometry to be open instead of periodic then this transition, which changes \mathbf{p}^{ν} to $(1/2, 0)$, leaves the outermost Wannier centers unpaired [red open circles in Fig. 6(b,c)] and pinned to the position $\nu_y = 0$. In contrast, the bulk Wannier centers are still free to move, and thus can adopt Wannier values that come in pairs $\nu, -\nu$ along both x or y .

We can verify this picture through the explicit calculation of the Wannier spectra of the DMQI for a cylindrical geometry in which boundaries are closed along x (y) and open along y (x) in which we calculate the Wannier values ν_x (ν_y). In Fig. 6(f) we see that all of the Wannier values come in $\pm\nu_i$ pairs, which matches our picture of having bulk Wannier functions with none isolated on the boundaries. In comparison we can look at Fig. 6(g), in which there is a pair of isolated Wannier values, for every unit cell along the y -direction, exactly pinned at $\nu_y = 0$. If we look at the eigenstates associated to these pinned Wannier values, we find that one set is localized at one of the open vertical edges, and the other set is on the other vertical edge. Notice, however, that since their values are pinned to $\nu_y = 0$, these edge Wannier states lie at the center of the unit cell in the direction parallel to the edge, and thus amount to a trivial edge polarization. Also, notice that such edge isolated Wannier states do not exist for the ν_x spectrum.

Now we can proceed with the deformation process along y . A second Wannier transition occurs between Fig. 6(d) and (e). At this transition, there is a gap closing in the x -Wannier bands at $\nu_x(k_y = \pi) = 1/2$, so that in Fig. 6(e) $\mathbf{p}^{\nu} = (1/2, 1/2)$. Notice the appearance of unpaired Wannier centers at the horizontal edges with Wannier values fixed to $\nu_x = 1/2$ [red solid circles in Fig. 6(e) along horizontal edges]. Simultaneously, the vertical edge states pinned at $\nu_y = 0$ that were isolated after the first Wannier transition undergo an *edge phase transition* that changes their value to $\nu_y = 1/2$ [red solid circles in Fig. 6(e) along vertical edges] (it must be a transition since the edge has reflection symmetry and thus ν_y for states on the edge is quantized to 0 or $1/2$). This is further confirmed by the explicit calculation of the Wannier spectrum on a cylinder shown in Fig. 6(h), which shows pairs of isolated Wannier values (per unit cell along the periodic direction) at both $\nu_x = 1/2$ and $\nu_y = 1/2$. If we look at the eigenstates corresponding to these isolated Wannier values we find that they are localized at the horizontal or vertical edges respectively. We emphasize that this last transition is the only one during this process that is accompanied by an edge phase transition which closes the edge energy gap, and that this transition is unavoidable along the vertical edges due to the fact that the isolated states (red) on the vertical edge constitute effective one-dimensional obstructed atomic limits protected by M_y symmetry.

A final remark is due regarding Fig. 6(e). The overall configuration of Wannier centers is such that reflection symmetries are preserved in the bulk, but not at the edges. In partic-

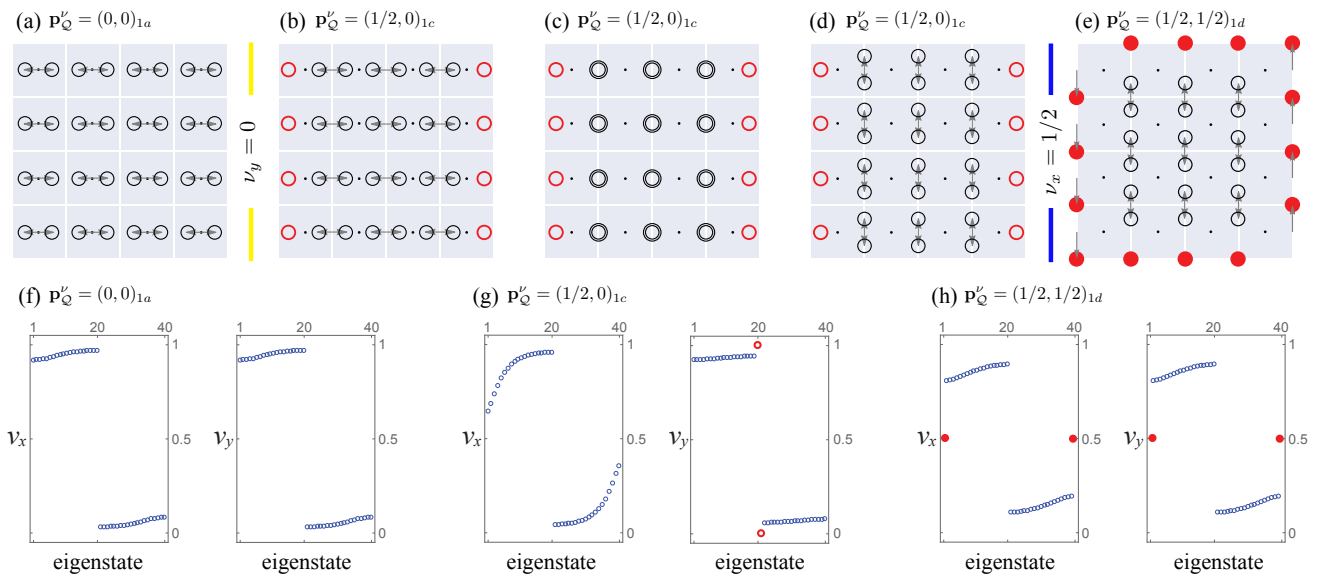


FIG. 6. Correspondence between real-space configurations and Wannier bands in the DMQI model, Eq. 1. (a-e) Wannier center location and nested (Wannier band) polarizations along a path illustrated schematically in Fig.5 (path 1). A Wannier gap closing transition happens between panels (a) to (b) at $\nu_y = 0$, and between (d) and (e) at $\nu_x = 1/2$. The latter happens at the Wannier chemical potential and corresponds to a boundary gap closing, and consequently to a topological phase transition. (f-h) Wannier spectra for cylindrical geometries for the three Wannier phases in (a-e). Wannier values in red have eigenstates that are localized on the edges of the cylinder. These results exactly match the configurations of the real space pictures in (a-e). The panels are labelled by the Wannier band polarization $\mathbf{p}_{\mathcal{Q}}^{\nu}$ where the subscript is an indication of the maximal Wyckoff position \mathcal{Q} that is associated to \mathbf{p}^{ν} . The arrows in (a-e) are drawn with their center at \mathcal{Q} as visual guide.

ular, it is not possible to maintain a symmetric configuration of Wannier centers for this system in an open boundary given the number of occupied states we need to fill the lower energy bands in periodic boundary conditions. This is an example of a filling anomaly where the condition of charge neutrality (integer band filling) is not compatible with the spatial symmetry [25]. We will provide a more detailed discussion of this important concept in the next subsection.

D. Corner charge and filling anomalies

1. Filling Anomaly

In the following, we would like to investigate possible physical signatures that distinguish the two different edge obstructed phases in the DMQI. As discussed briefly in Sec. II A, the $\mathbf{p}^{\nu} = (1/2, 1/2)$ phase exhibits zero energy corner modes, but only when particle-hole or chiral symmetries are present. In the absence of these symmetries, these corner states are not pinned to zero energy and, as a result, can be moved up and down in energy, though they remain degenerate because of the spatial symmetry. Once they are pushed to the conduction or valence band they can hybridize with the delocalized states there, and do not necessarily remain exponentially localized at the corners. Thus, the edge obstructed phase $\mathbf{p}^{\nu} = (1/2, 1/2)$ is not associated with corner modes in general.

The absence of zero-energy corner modes, however, does not mean that other signatures such as corner *charges* (rather than states) are absent. To investigate this possibility, let us

start with the particle-hole/chiral symmetric case and then add terms that break these symmetries. We note that the DMQI has $4N$ states in total, where N is the number of unit cells. In the particle-hole/chiral symmetric case, we know there are 4 zero-energy corner states leaving $2N - 2$ states in both the conduction and valence bands. Once particle-hole/chiral symmetry is broken, the corner states can move in energy but they remain degenerate due to mirror symmetries, leading to two possibilities: they either remain inside the gap or move into the valence or conduction band. In the first case, they remain localized eigenstates of the Hamiltonian having degeneracy protected by the two mirror symmetries. As a result, the system can not be gapped⁵ at half-filling since there are two electrons that need to occupy four degenerate states.⁶ In the second case, these states hybridize with the states in the valence (conduction) band forming new and more extended eigenstates. As a result, the number of states in the valence (conduction) band is changed to $2N + 2$, and the chemical potential will lie in the valence (conduction) band at half filling which implies that the system is again not gapped. This phenomenon, in which it is impossible for a system to be simultaneously gapped, symmetric, and charge-neutral at a certain filling has recently been referred to as “filling anomaly”

⁵ A gapped system is one with no charge excitations at zero or infinitesimally small energy.

⁶ We note that the usual paradigm of slightly breaking the symmetry so that two out of four modes could be filled is unavailable as we are strictly enforcing the symmetry. Indeed filling the modes this way essentially results in spontaneous symmetry breaking in the thermodynamic limit.

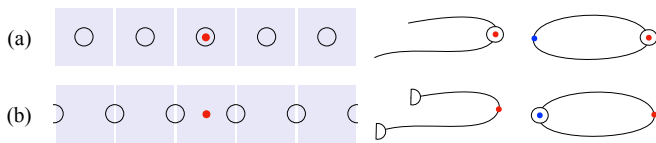


FIG. 7. Bulk obstruction and filling anomaly in an SSH chain protected by inversion symmetry. With open boundaries there is a single inversion center (red dot), while when the boundaries are identified an antipodal inversion center is created at the stitching point (blue dot). (a, left) Trivial state: the filling of the inversion center (red dot) is odd just as the total filling of the chain is odd, which implies the electrons can be filled while preserving inversion. (a, right) When the end points are identified only the red inversion center is filled. (b, left) Nontrivial state: at an odd filling, if the red inversion center is not filled there is no way to fill the chain while preserving inversion, and there is a filling anomaly associated with end charges that need to be fractional at neutrality to preserve the symmetry. (b, right) Identifying the end points cures the anomaly, i.e., we no longer require fractionalization at neutrality, and only the blue inversion center is filled. With open boundaries the two phases can be distinguished by the endpoint charges, while with closed boundaries a topological distinction remains since the charge at the blue site cannot be moved to the red site while preserving both the symmetry and the bulk gap. This is an example of a bulk obstruction.

[25, 38]. If we impose the conditions that the system is a symmetric gapped insulator, then the filling anomaly will manifest in excess or deficient charges distributed symmetrically in the four corners. For the DMQI, such charge is equal to $(n + e/2)$ per corner for some integer n ⁷.

2. Real space understanding of filling anomalies

We now present an alternative understanding of the filling anomaly in the DMQI model which will enable us to study filling anomalies in more general models in two and three dimensions. First, we note that, in general, when we consider a system with open boundaries, lattice translations are absent and the symmetry of the system is restricted to the point group G with respect to the symmetry center \mathcal{O} of the entire sample. Each Wannier state is part of a Wyckoff position \mathcal{Q} whose orbit may extend across the entire sample (illustrated for the DMQI in Fig. 8). Before considering the DMQI model, let us begin by considering the simpler example of the 1D SSH chain with inversion symmetry.

Imagine we start with an SSH chain having N unit cells (with two orbitals per unit cell) at half-filling so that the total number of electrons is N . We will now show that, in some cases, it is impossible for this system to be gapped, inversion-symmetric, and charge-neutral when considered with open boundaries. Our proof proceeds by assuming that such a

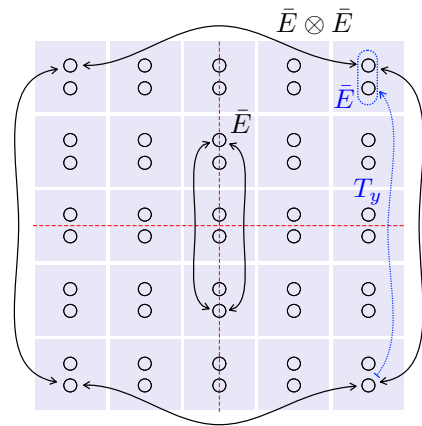


FIG. 8. Symmetry representations of the DMQI model. The open circles indicate the positions of the Wannier centers in a given basis, and the grey squares represent the unit cells. On a torus the symmetry is $D_2^\pi \times T^2$, and every two electrons in each unit cell are symmetry related (by reflection and subsequent translation). Together they form an \bar{E} representation of D_2^π (enclosed in a dashed blue oval). With open boundaries only the point-group D_2^π is preserved and the Wannier centers form symmetry orbits indicated, for a few cases, by the black arrows. If a Wannier center lies in a general Wyckoff position with multiplicity four, it is part of a reducible $\bar{E} \otimes \bar{E}$ representation of D_2^π . Wannier centers on high symmetry lines form 2D irreducible representations \bar{E} .

gapped, charge-neutral atomic insulator exists and deriving a contradiction. We start by noting that, due to inversion, all electrons in the open system are either localized at the inversion center \mathcal{O} or at inversion-related pairs of points relative to it. These pairs can be symmetrically moved to the center \mathcal{O} without breaking the symmetry or closing the gap, which means that our system can be symmetrically deformed to an insulator with all electrons at the inversion center. Note, however, that such a process never changes the initial parity of the filling at the center $\nu_{\mathcal{O}}$ since it always adds an even number of electrons. This leads to a contradiction if the parity of $\nu_{\mathcal{O}}$ at the beginning (for the periodic system) differs from that of N ; we cannot symmetrically move all the states to the center in this case. This means that one of our assumptions: symmetry, charge-neutrality, or an insulating gap does not hold in this case, hence reflecting the existence of a filling anomaly. One way to intuitively understand the filling anomaly is to see that at a filling corresponding to neutrality an electron would be forced to fractionalize into two pieces to preserve the inversion symmetry, as illustrated in Fig. 7. If we require that the system be neutral then the filling anomaly in the SSH chain generates the bulk polarization, i.e., it implies that the inversion symmetry will be broken spontaneously and a dipole moment will appear that creates opposite fractional charges of $\pm e/2$ bound at the two edges. If we require that the system remains symmetric then it will either be gapless since there will be degenerate low-energy modes, or we will need to add an extra electron (at the minimum), which will violate neutrality.

A similar analysis can be performed for the DMQI model.

⁷ Corner charges associated with filling anomalies are only defined modulo an integer charge since we are free to add integer charges to the corners while keeping the system a symmetric insulator.

We start by considering $N_x N_y$ unit cells at a filling of two electrons per unit cell. With open boundaries, the symmetry group of the model is the point group D_2^2 relative to \mathcal{O} , with irreducible representations given in Appendix A, Table II. Similar to the discussion on the SSH, we assume the system is a symmetric charge-neutral atomic insulator to derive a contradiction⁸. Since the mirror symmetries anticommute, the electrons at the center \mathcal{O} , which is fixed by both mirrors, transform under the 2D irreducible representation \bar{E} . The electrons on the $x = 0$ or $y = 0$ mirror lines come in pairs, related by M_y or M_x respectively, that also transform under \bar{E} . The electrons in the general Wyckoff position $(\pm x, \pm y)$ come in groups of 4, which transform under the reducible representation $\bar{E} \otimes \bar{E}$, which can be decomposed into a sum of four 1D irreducible representations $A_1 \oplus A_2 \oplus B_1 \oplus B_2$ as shown in Fig. 8. This implies that the total bulk filling is necessarily even. Let us denote the total number of states at high symmetry points (i.e., either at the center \mathcal{O} or on one of the mirror lines) by ν_S . We note that ν_S can be changed by symmetrically moving states from the general Wyckoff position, but its value modulo 4 remains the same. In addition, we note that ν_S is always even since the filling of the center \mathcal{O} is always even due to mirror anticommutation (actually ν_S corresponds precisely to twice the number of \bar{E} representations in the system since the orbitals in the general Wyckoff position can be decomposed into 1D irreps). Thus, if $\nu_S/2$ has a different parity compared to $N_x N_y$, it is impossible to bring all the states to a high symmetry point (either at the center \mathcal{O} , or at one of the mirror lines) indicating the presence of a filling anomaly where, at neutrality, a pair of electrons is symmetrically split among the four corners. This filling anomaly diagnoses the bulk quadrupole moment in the system.

We remark that this is not the only possible filling anomaly for this point-group. If we allow for additional bands transforming under 1D representations (for which mirrors commute), then the total bulk filling can be odd⁹. This leads to an additional possible filling anomaly diagnosed by the parity of the full filling at the origin $\nu_{\mathcal{O}}$. This type of filling anomaly reflects a bulk obstruction, just like it does for the 1D SSH chain, and diagnoses the sum of the polarizations along the x and y directions, each of which must be quantized by the mirror symmetries. To resolve individual x and y polarizations, we would need to consider cylindrical geometries with an open boundary along one of the directions and a periodic boundary along the other.

3. Filling anomalies for edge vs bulk obstructions

The discussion of the previous two sections regarding filling anomalies did not clarify the distinction between filling

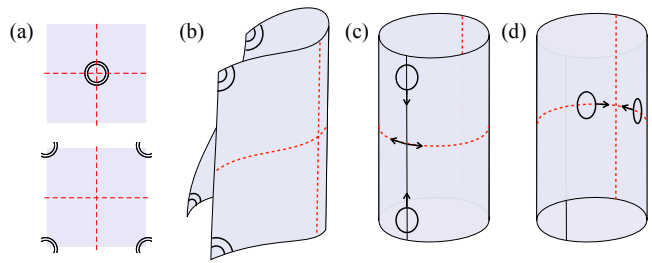


FIG. 9. Sewing the boundaries in a boundary obstructed atomic insulator (e.g., the DMQI quadrupole insulator). When the boundary is stitched along one direction the filling anomaly is lifted since the two corners contribute with half a charge so that all sites have integer filling. Interestingly, in this case the bulk obstruction is also lifted: The seam line is a high-symmetry line where the two states can freely move towards each other and symmetrically reach all maximal Wyckoff positions, including the original symmetry origin marked with a red dot.

anomalies in edge-obstructed models like the DMQI, compared to bulk-obstructed models such as the SSH chain. Our goal in this subsection is to elucidate this difference. The distinction can be understood by studying what happens when the anomaly is resolved by identifying some of the edges of the open system. What we mean by “resolve” is that the change of geometry now allows for a symmetric, gapped, and neutral configuration at our filling of interest. For example, in the SSH case, we can resolve the anomaly by identifying the two endpoints, which become a new inversion center \mathcal{O}' . In this case, it is possible to have a symmetric, charge-neutral insulator whose filling N has different parity from $\nu_{\mathcal{O}}$ since there is now a new inversion center that can compensate for the parity mismatch. In the phase with (without) the filling anomaly, the new inversion center \mathcal{O}' will have an odd (even) filling whose parity cannot be changed by symmetrically adding or removing electrons. Thus, the filling anomaly in the open system corresponds to a bulk topological distinction in the periodic system, i.e., the anomaly can be resolved by identifying opposite edges, but the resulting insulator is topologically non-trivial (i.e., an obstructed atomic limit).

We can similarly resolve the filling anomaly of the DMQI by identifying either pair of opposite edges. When the boundary is stitched together, the symmetry of the corner and the seam line is enhanced compared to the open geometry. The filling anomaly is resolved following this boundary identification since only two electrons (transforming under \bar{E}) are required to fill the edge states after the stitching, as illustrated in Fig. 9. Another way to say this is that there is a new high symmetry line (invariant under M_x or M_y depending on the identified edges) whose filling can compensate for the mismatch between ν_s and $2N_x N_y$ modulo 4. However, in contrast to the SSH chain, the resulting system is completely trivial since the two electrons at the edge can now be symmetrically moved to the original center \mathcal{O} . The reason is that, unlike the SSH case, the high symmetry positions at the center \mathcal{O} , or at any mirror line, are all connected. Thus, the difference between filling anomalies associated with boundary

⁸ Note that here we need the extra assumption that the system is an atomic insulator, i.e., it admits a Wannier representation, which was not needed in the 1D case since all 1D systems are Wannier representable.

⁹ Here, we take the point of view that the point-group is fixed to be D_2^2 , but the electrons can transform in any of its representations even those where mirrors commute.

and bulk obstructions is that the former leads to completely trivial bulk phases, whereas the latter leads to topologically non-trivial bulk phases when the anomaly is resolved by identifying some of the edges.

One final remark concerns the effect of adding some extrinsic degrees of freedom at the edge of the DMQI. For example, we can add an SSH chain with N_{SSH} lattice sites to one edge (say the one parallel to the x -axis), and its mirror image to the opposite edge. This process changes the total number of states by $2N_{\text{SSH}}$. It also introduces $2\nu_{O,\text{SSH}}$ states at the $y = 0$ mirror line, where $\nu_{O,\text{SSH}}$ is the filling at the center of each SSH chain. This changes the number of states on the mirror lines in the DMQI, and as a result, if the SSH chain has a filling anomaly indicated by parity mismatch between N_{SSH} and $\nu_{O,\text{SSH}}$, then its addition to the DMQI in the anomalous (non-trivial) phase will remove the filling anomaly of the DMQI. Such a process will, however, induce a filling anomaly in the non-anomalous (trivial) phase. Thus, the effect of symmetrically adding SSH chains at the edge essentially exchanges what we would identify as the trivial and non-trivial phase, but keeps the distinction between them. As we will see later, this is a general feature for edge-obstructed phases.

III. BOUNDARY OBSTRUCTIONS: GENERALITIES

A. General definition

After discussing the properties of the DMQI model in detail, our goal now is to introduce a general definition to capture topological distinctions encoded in a boundary obstruction rather than a bulk obstruction. Before introducing the definition, let us recall some relevant concepts. Given a Hamiltonian \mathcal{H} and a chemical potential μ , we can define the projector on the filled bands via

$$P = p(\mathcal{H}, \mu) = \sum_{\epsilon_n < \mu} |\psi_n\rangle \langle \psi_n|, \quad \mathcal{H} |\psi_n\rangle = \epsilon_n |\psi_n\rangle. \quad (4)$$

The projector $p(\mathcal{H}, \mu)$ is well-defined if and only if there are no eigenstates of \mathcal{H} at the chemical potential, i.e., only if \mathcal{H} is gapped at μ . We then consider a canonical procedure to implement a surface termination which does not depend on P as follows. We specify a real scalar function $\phi(\mathbf{r})$ that reduces to the constants $\phi_{\text{in}} < \mu$ deep inside the sample and $\phi_{\text{out}} > \mu$ far outside the sample (see the discussion of Sec. II C and Fig. 4). A surface termination is implemented by replacing the bulk projector P with $P(\mathbf{r})$ defined as

$$P(\mathbf{r}) := p(P\phi(\mathbf{r})P + \phi_{\text{out}}(1 - P), \mu) \quad (5)$$

which reduces to P deep inside the sample and to the trivial projector (where all states are empty) far outside the sample. We note that defining our surface termination in terms of a $\phi(\mathbf{r})$ -dependent auxiliary Hamiltonian is *not* the same as adding an edge potential $V(\mathbf{r}) = \phi(\mathbf{r})$ for which the surface termination would instead be implemented as $P(\mathbf{r}) = p(\mathcal{H} + V(\mathbf{r}), \mu)$. The way we chose to implement the termi-

nation (5) has the advantage of connecting directly to the Wannier spectrum. It should be noted, however, that our definition of BOTPs below only relies on the existence of a canonical way to implement a surface termination, i.e., a way to keep a surface termination fixed while we deform the Hamiltonian, regardless of which specific implementation we choose.

To study the surface spectrum in a given surface termination, we consider the spectrum of the operator $P\phi(\mathbf{r})P + \phi_{\text{out}}(1 - P)$, where the filled bulk states accumulate at ϕ_{in} , and the empty states deep inside or outside the sample accumulate at ϕ_{out} . The energy eigenvalues in-between ϕ_{in} and ϕ_{out} correspond to eigenstates localized close to the surface and their dispersion, as a function of the momentum tangent to the surface, yields the surface spectrum at a given point.¹⁰

For a given (tight-binding) Hamiltonian $\mathcal{H}(\mathbf{k})$ describing a periodic translationally-symmetric system, the implementation of the surface termination described by Eq. 5 goes as follows. We start by constructing the projection operator P onto filled bands in momentum space and then we Fourier transform to real space before substituting the projector into Eq. 5. The surface spectrum is given by the eigenvalues of the real-space operator $P\phi(\mathbf{r})P + \phi_{\text{out}}(1 - P)$. We note that this procedure was used to generate the edge spectrum in Fig. 4 for the DMQI Hamiltonian (1) with the edge termination described by the potential (3).

To define boundary topological obstructions, we consider two projectors P_1 and P_2 defined for a periodic system which are invariant under a symmetry group G containing internal and point group symmetries relative to a given point \mathcal{O} ¹¹. We say there is a boundary obstruction between P_1 and P_2 if (i) there is a smooth trajectory in the space of symmetric projectors $P(t)$ for $t \in [0, 1]$ connecting P_1 and P_2 such that $P(0) = P_1$ and $P(1) = P_2$, and (ii) there is a symmetric surface termination for which any such trajectory $P(t)$ necessarily closes the energy gap at a high-symmetry point (HSP) of the surface. An HSP is a point that is left invariant by at least one non-trivial point group symmetry in G . Our definition means that for each symmetric smooth trajectory connecting P_1 and P_2 , there exists an HSP whose spectrum is gapped for P_1 and P_2 , but gapless for at least one point along the trajectory. One important subtlety in this definition is the requirement that the surface termination is fixed along the trajectory. This means that, given a trajectory $P(t)$ in the periodic system, the corresponding trajectory in the open system is $P(\mathbf{r}, t) = p(P(t)\phi(\mathbf{r})P(t) + \phi_{\text{out}}[1 - P(t)], \mu)$ where $\phi(\mathbf{r})$ does not depend on t . This ensures that any surface gap closing is driven by changes in the bulk parameters. We note here that the ability to assign a surface gap closing to changes in the

¹⁰ We will generally identify the spectrum at a point on the surface of a d -dimensional system with the spectrum at the tangent $(d - 1)$ -dimensional hyperplane as in Refs. [21, 23]. This is only problematic at sharp intersections of several hyperplanes, e.g., hinges where the tangent plane is not well-defined. In this case, we can restrict ourselves to the dispersion along directions where tangent vectors are defined, e.g., the direction along the hinge.

¹¹ There may be additional translation symmetries present, but they are not needed for our definition.

bulk parameters relies crucially on the existence of a canonical way to implement surface terminations like the one defined by Eq. 5 for which the notion of changing the bulk Hamiltonian while fixing the boundary termination is meaningful.

Our definition distinguishes different classes of Hamiltonians based on boundary obstructions, and enables a finer distinction between phases that are topologically identical from the perspective of bulk topology. We will call such classes boundary-obstructed topological 'phases' (BOTPs). We reiterate here that BOTPs are not phases in the standard sense since they are not distinguished by bulk phase transitions with periodic boundary conditions. In general, boundary obstructions may co-exist with bulk obstructions. For instance, a non-trivial bulk phase, such as a 3D HOTI with chiral hinge states, can have several distinct patterns of hinge states that differ by boundary obstructions. However, we note that we can always move between such different surface configurations by adding a BOTP. Such a BOTP, which is manifestly trivial in the bulk, can be identified with the *difference* between the Hamiltonians corresponding to the two distinct patterns of surface states. Thus, when studying boundary obstructions, we can restrict ourselves to phases that are completely trivial in the bulk.

One important aspect in our definition is that only gap-closings at high-symmetry points on the boundaries are relevant. This requirement, which may seem unnecessary at first glance, is crucial for our definition to make sense. To illustrate the need of such a distinction between a gap-closing at high-symmetry points vs. generic points, let us consider the DMQI on a disk geometry whose boundary is a circle. If chiral/particle-hole symmetry is unbroken, the $(1/2, 1/2)$ phase of the model is characterized by four symmetry-related zero-energy states. These states can be associated with domain walls for a surface Dirac mass [21, 23, 38] that is invariant under both mirrors and changes sign four times as we go around the circle (cf. Fig. 10).¹² In this case, we can see that the gap at any generic point on the edge can be closed by simply moving one of the domain walls through this point. This gap-closing cannot be associated with a topological distinction since that would imply the existence of uncountably-many distinct topological phases associated with all possible (continuously varying) positions of the domain walls. On the other hand, by restricting ourselves to gap-closing transitions occurring at the HSPs at $x = 0$ or $y = 0$, we can distinguish between the cases with and without corner states. This follows because the only way to get rid of the zero-energy domain wall states is by annihilating them pairwise at one of the mirror invariant points at the boundary. Another way to see this is by recalling the discussion of Sec. IID, in which the filling anomaly in the DMQI was diagnosed by the mismatch between the total filling and the number of states lying at the

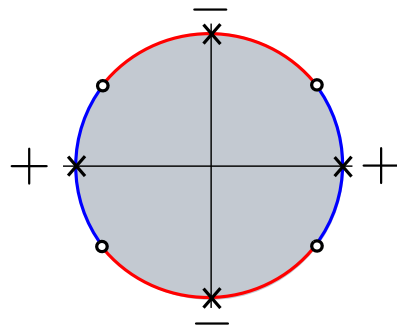


FIG. 10. Illustration of zero-energy states (open circles) for the chiral-symmetric DMQI model on a circle geometry. Zero energy states are localized on domain walls for an edge mass term that is invariant under the two mirror symmetries, but has a different sign at the $x = 0$ and $y = 0$ lines, thus changing sign four times along the edge. These zero-energy states can only be removed by annihilating pairwise at the high symmetry points denoted by the x symbol.

two mirror lines modulo 4. Thus, an edge gap-closing can change the filling anomaly by changing the number of states at the mirror lines if and only if this gap-closing occurs at one of the mirror invariant points at the edge. This means that our definition captures the same topological distinction captured by the filling anomaly for the DMQI.

1. Relationship to HOTIs

It is instructive to relate our understanding of the boundary obstruction in the DMQI in terms of surface domain walls to the corresponding understanding in HOTIs pioneered in Refs. [20, 21, 23, 38]. In these works, the surface states of HOTIs were understood in terms of symmetry-enforced surface domain walls where the transformation properties of the surface Dirac mass under spatial symmetry forced it to change sign. In the DMQI, the surface mass does not change sign under either mirror symmetry. However, by requiring the edge spectrum to be gapped at HSPs, we can distinguish phases based on the sign of the mass term at these points which are associated with different patterns of surface domain walls. For instance, if the sign of the mass term at $x = 0$ differs from that at $y = 0$, then there are four domain walls as we go around the circle (cf. Fig 10), which cannot be removed without changing the sign of one of these masses. Thus, we can understand the localized boundary modes of the DMQI as domain walls protected by the gap at HSPs. We note that the transformation properties of the surface mass term under the symmetries does not force it to change sign. Instead, two distinct, symmetry-allowed configurations of mass signs at HSPs are possible, but they cannot be deformed to each other (without closing a gap at an HSP). This is in contrast to HOTIs where the sign change of the mass is enforced by the symmetry.

It is worth noting that our topological distinctions are similar to a real-space version of those used in diagnosing semimetals whose spectrum is gapped at high-symmetry momenta [39, 40]. For instance, a Weyl semimetal with two

¹² One way to see that this has to be the case is to start with the C_4 symmetric case, which is a proper HOTI whose surface states are symmetry-enforced domain walls [21, 23], and then imagine breaking C_4 . The local stability of the corner states is only protected by the local symmetries (chiral symmetry in this case) but we can now move them away from the C_4 -symmetric positions at the corners.

inversion-related Weyl points with opposite chirality can be smoothly deformed to a trivial insulator by bringing the two Weyl points together. However, this process will necessarily involve a gap-closing at one of the inversion-invariant momenta [41, 42].

Another related concept is that of the so-called extrinsic HOTIs discussed in Refs. [22, 24]. These are insulators hosting “higher-order” surface states with co-dimension $(d - D)$ ($D > 1$) that can be removed by symmetrically adding a lower-dimensional SPT on the boundary. Our boundary-obstructed phases fall under this definition since their surface states (or filling anomalies) can be removed by adding some SPTs on the boundary while preserving the symmetry. For example, the corner modes (and corner charge) in the DMQI can be removed by symmetrically adding a pair of SSH chains at two symmetry-related edges as discussed in Sec. IID. However, for a BOTP such a process only redefines what we identify as the trivial phase, and *does not* remove the distinction between different phases. In other words, the *relative* distinction between the phases is insensitive to what we add at the boundary as long as it is kept fixed when comparing the two phases, a requirement that is already encoded in our definition. Thus, we only consider boundary transitions driven by changes in the bulk, ruling out the cases in which a non-trivial SPT is glued to the surface of a trivial bulk.

In general, relative topological distinctions are captured by a mathematical structure called a *torsor* (rather than a group) [43]. A torsor can be thought of as a group without a clear notion of an identity element (trivial phase). We notice that this concept is not new as many topological distinctions for well-known bulk phases are also relative. This is the case, for example, for obstructed atomic phases where an arbitrary choice is made for the *trivial* atomic limit [29, 39]. A simple example is provided by the 1D SSH chain which has two different values of the polarization that can only be distinguished relative to each other. Such a relative distinction can be made more absolute by taking into account the background of positive ions or fixing a convention for the unit cell, either of which can be used to distinguish the two polarization states in the SSH chain according to whether the charge centers lie on top of the positive ions (center of the unit cell) or not (edge of the unit cell)¹³. It is, however, important to keep in mind that the topological distinctions in the electronic Hamiltonian (which does not contain information about the positive ions) in these cases are strictly relative.

2. Diagnosing BOTPs using Wannier spectrum

We now turn to a discussion of how the Wannier spectrum can be used to diagnose BOTPs. Let us first recall some basic facts about the Wilson loop operator. The Wilson loop operator $\mathcal{W}^b(\mathbf{k}_0)$ is a unitary operator defined by parallel transporting the occupied-band projection operator from a point \mathbf{k}_0 to

$\mathbf{k}_0 + \mathbf{b}$ along the reciprocal lattice vector \mathbf{b} . Its eigenvalues have the form $\exp\{2\pi i \nu_b(\mathbf{k}_\perp)\}$, and its eigenstates are the hybrid Wannier functions that are localized in the direction along the lattice vector $\tilde{\mathbf{b}}$ which is dual to \mathbf{b} , (i.e. $\tilde{\mathbf{b}} \cdot \mathbf{b} = 2\pi$, $\tilde{\mathbf{b}} \cdot \mathbf{k}_\perp = 0$) for a fixed momentum along the perpendicular directions \mathbf{k}_\perp [30, 31]. The dispersion of $\nu_b(\mathbf{k}_\perp)$ with \mathbf{k}_\perp is known as the Wannier spectrum, and provides information about the \mathbf{k}_\perp -resolved center of the charge along the $\tilde{\mathbf{b}}$ direction. The Wannier spectrum is only defined modulo 1 which reflects the periodicity of the lattice along $\tilde{\mathbf{b}}$.

To see how boundary obstructions can be diagnosed using the Wannier spectrum, we note that since we only care about gaps at HSPs, we can restrict ourselves to boundary terminations consisting of intersections of $(d - 1)$ -dimensional high-symmetry hyperplanes to study a d -dimensional BOTP (a high-symmetry surface hyperplane is one which is left invariant by at least one non-trivial spatial symmetry). We can then study the surface spectrum at different surface hyperplanes, or at the intersection of any number of such hyperplanes. For example, in three dimensions, we can consider the spectrum at 2D surfaces or 1D hinges lying at the intersection of two such surfaces. In the following, we focus on boundary obstructions accompanied by a gap-closing at a surface hyperplane (i.e., surface obstructions) rather than the intersection of surface hyperplanes (i.e., hinge obstructions). For these types of geometries, condition (ii) in our definition is equivalent to the statement that any trajectory connecting the two d -dimensional BOTPs must close the surface gap for at least one high-symmetry surface hyperplane. The spectrum of a surface hyperplane perpendicular to a lattice vector $\tilde{\mathbf{b}}$ is known to be continuously deformable to the Wannier spectrum $\nu_b(\mathbf{k}_\perp)$ [37](see discussion of Sec. IIC). In the following, we will assume that such a continuous deformation between the surface spectrum and the Wannier spectrum can be done *without* closing the gap at the chemical potential. This can be used to define a Wannier chemical potential μ_b at which the Wannier spectrum $\nu_b(\mathbf{k}_\perp)$ is gapped. Thus, we can identify actual surface gap-closing transitions in a surface hyperplane perpendicular to the vector $\tilde{\mathbf{b}}$ with gap-closing transitions in the Wannier spectrum $\nu_b(\mathbf{k}_\perp)$ at the WCP μ_b . Unless otherwise stated, we choose a convention that the boundary termination is consistent with the unit cell. The boundaries of the unit cell are chosen to be at 1/2 in units of the primitive lattice vectors, which corresponds to a Wannier chemical potential $\mu_b = 1/2$ for any primitive lattice vector $\tilde{\mathbf{b}}$.

The discussion above provides a recipe for diagnosing boundary obstructions by using Wannier spectra as follows. Given two bulk Hamiltonians and a surface termination specified by a set of WCPs μ_b , a boundary obstruction is established if every trajectory connecting the two Hamiltonians involves a gap closing for one of the Wannier spectra $\nu_b(\mathbf{k}_\perp)$ at the WCP μ_b . If there is not such a Wannier gap closing then that particular choice of surface termination does not exhibit a boundary obstruction, but that does not preclude another distinct termination from supporting one.

¹³ We note that there is still an integer ambiguity in defining polarization coming from the freedom to assign the electron position to any unit cell.

B. Band representations of BOTPs

To aim for a general classification of boundary obstructed topological phases it is convenient to relate our discussion to the formalism developed for topological quantum chemistry in Refs. 29 and 36. In these works, the concept of band representations was used to incorporate both the symmetries and momentum space Berry-Zak phases of band Hamiltonians into a single formalism. Such band representations correspond to the possible atomic limits, or Wannier representable phases, allowed for the different space groups. We provide a brief introduction to this formalism in Appendix C with a focus on the concepts we apply here. When the ground state of a Hamiltonian can be described by exponentially localized Wannier functions, the set of Wannier functions are described by a band representation ρ^k . Band representations can be decomposed into a direct sum of elementary band representations (EBRs) that have been exhaustively classified. Energy bands that cannot be disconnected into subsets represented by exponentially localized Wannier functions are, to a more strict sense, topological, though we will sometimes call obstructed atomic limits topologically non-trivial, in-line with a more conventional usage. Although we are not interested in giving a complete classification of BOTPs, here we convey how an approach using band representations can be used to capture boundary obstructions. An advantage to this approach is that it is insensitive to the details of the Hamiltonian, and any considerations using this formalism are not modified under adiabatic deformations of the Hamiltonian which preserve the symmetry and energy gap.

In our definition of BOTPs we have restricted ourselves to phases that do not have a bulk obstruction, which implies that all bulk phases under consideration are described by a band representation. Equivalent band representations, for a symmetry group $G \times T^d$, share the same symmetry representations at high symmetry points in both momentum (Bloch basis) $\Lambda_K = \rho^k \downarrow G_K$, where G_K is the little group at the Brillouin zone point K , and in real space (Wannier basis) $\Lambda_q = \rho^k \downarrow G_q$ ¹⁴ with G_q the site symmetry group of the real space position q . For example, in the DMQI model all four $\mathbb{Z}_2 \times \mathbb{Z}_2$ classes that are separated by Wannier gap closings correspond to the equivalent bulk band representations. This means that there exists a smooth, unitary, matrix-valued function that transforms the representations of the four different classes into each other (we provide explicit details of this mapping in App. C). Using the DMQI model, we have motivated in Secs. IIB and IIC that adiabatic, symmetry-preserving paths that exist between different Hamiltonians with periodic boundary conditions can be obstructed in the presence of a boundary. Thus, band representations that are equivalent in periodic boundary conditions may be inequivalent in the presence of a boundary. Indeed, from the real-space analysis in Sec. IIB and the Wannier band analysis in

Sec. IIC, we showed that one out of the four classes of the DMQI can be cut-off and distinguished from the other three in the presence of open boundary conditions. In this subsection, we formally characterize this type of obstruction in the context of band representations.

1. Wannier band representations

Consider a bulk system described by a band representation ρ^k of $G \times T^d$. The bands forming the Wannier spectrum of \mathcal{W}^b only transform under a subgroup of the full space group since a particular family of planes, normal to the reciprocal vector \mathbf{b} , is chosen in which to maximally localize the Wannier functions. This subspace preserves a point group $G^b \subseteq G$, and translations $T^{d-1} \subset T^d$. It is natural to define the *Wannier band representation* w^{b,k_\perp} (WBR) by the subduction of the band representation to the subgroup preserved by the Wannier spectrum. This is exactly the subgroup preserved by the respective (ideal) boundary normal to \mathbf{b} , hence we have

$$w^{b,k_\perp} = \rho^k \downarrow (G^b \times T^{d-1}). \quad (6)$$

Notice that k_\perp in the WBR takes values in only the $d - 1$ dimensional Brillouin zone transverse to \mathbf{b} , we will however omit the \perp subscript for simplicity in the notation.

Since the symmetry group of \mathcal{W}^b is smaller than the bulk symmetry group, the connectivity of the bulk band representation ρ^k is not generically preserved by the subduction. Thus, even when ρ^k is a connected elementary band representation, $w^{b,k}$ does not need to be. The WBR can generally be decomposed into the direct sum of disconnected components that correspond to distinct connected sets of Wannier bands labelled by an index a ,

$$w^{b,k} = \bigoplus_a w_a^{b,k}. \quad (7)$$

This construction defines a notion of topological distinctions for the Wannier bands i.e., two WBRs $w^{b,k}$ and $\tilde{w}^{b,k}$ are equivalent if and only if they have equivalent decompositions in terms of disconnected components $w_a^{b,k}$, not all of which have to be elementary WBRs. *A crucial observation is that the subduction-decomposition does not necessarily yield the same set of disconnected components for bulk band representations ρ^k that are equivalent to each other.* This means that phases that can be smoothly deformed to each other in the bulk, and are thus equivalent from the bulk perspective, may correspond to distinct WBRs. Indeed, as we have already seen for the DMQI, a connected set of bulk energy bands yields a set of two disconnected Wannier bands (separated by a gap around $\nu = 0$ and $\nu = 1/2$). This set of disconnected bands are classified by a $\mathbb{Z}_2 \times \mathbb{Z}_2$ topological distinction, and the WBR depends on the bulk parameters of the Hamiltonian, despite descending from equivalent bulk BRs.

As we have stressed in the previous sections, closing the gap of the Wannier spectrum does not imply closing the gap at a boundary. This means that the topological distinctions of WBRs encoded in (7) do not necessarily translate to boundary

¹⁴ Here, \downarrow indicates subduction of the representation to the succeeding subgroup.

topological distinctions. To make connection to the boundary spectrum, we have to also assume that the different disconnected components of a WBR are separated by Wannier gaps, which is always possible. Once the different disconnected components of the Wannier bands are separated by Wannier gaps, boundary topological distinctions are defined by identifying equivalence classes of WBRs under smooth symmetric deformations that do not close the Wannier gap *at the Wannier chemical potential* μ_b . The determination of the WCP corresponding to a given surface termination was described in detail for the DMQI in Sec. II C, and for the general case in Sec. III A. Within the band representation picture, the WCP can be seen as an external piece of information specifying a boundary termination. This means that changes in the WBR decomposition accompanied by Wannier gap closings away from the WCP can occur, but they correspond to the same topological phase, and, importantly, do not differ in their boundary signatures. Physically, such processes correspond to mixing the boundary degrees of freedom and those deeper in the bulk without going through a gap-closing at the physical boundary. This provides a procedure to reduce the Wannier topological distinctions (which correspond to $\mathbb{Z}_2 \times \mathbb{Z}_2$ for the DMQI) to boundary topological distinctions (which corresponds to \mathbb{Z}_2 in the DMQI) for a given boundary choice, based on whether the Wannier gap closings generate an actual boundary energy gap closing or not. Two phases that are equivalent in the bulk and on the level of surface obstructions may still be distinguished by a higher order boundary obstruction, e.g., a hinge obstruction. Diagnosing such obstructions requires considering higher-order Wannier spectra. The discussion is conceptually similar to the one relating Wannier spectra to surface spectra, hence we will not provide a detailed description of it here. We do note that there is an additional complexity since there are now two distinct higher-order Wannier spectra that correspond to a single hinge.

C. Boundary signatures

Although the notion of boundary obstruction, as we have defined it, captures a relative distinction between phases, we can ask whether such a relative distinction is associated with an observable boundary signature. For example, the two boundary obstructed phases of the DMQI differ by the existence of a filling anomaly. In the following, we will investigate the possible boundary signatures (surface states or filling anomalies) associated with boundary obstructions in a general setting.

To this end, it is instructive to recall how boundary signatures arise in standard (bulk) topological phases. Topological phases in a free fermion system can be grouped into three categories: (i) those associated with anomalous surface states¹⁵, (ii) those associated with a filling anomaly, or (iii) those that

are not accompanied by surface states or filling anomalies. We note that topological phases in (ii) can be associated with zero-dimensional edge or corner states in the presence of particle-hole or chiral symmetry.

Examples of (i) include common topological phases such as Chern insulators, whereas (ii) includes, for instance, topological crystalline phases with non-vanishing charge polarization which are associated with surface charges rather than surface states, e.g., an inversion-symmetric SSH chain. Case (iii) is not associated with any boundary signature. As such, it is much more difficult to distinguish trivial and non-trivial phases because the relative distinction is captured only by changes in the symmetry representations of the filled bands. For example, we can think of two different SSH chains, each with a single electron per unit cell, and such that the charge center in both cases is at 0, but the orbital character is different under inversion (e.g., s vs p orbitals corresponding to ± 1 inversion eigenvalues). These two cannot be deformed to each other without breaking inversion symmetry, but this obstruction is not associated with any topological boundary signature.

Now let us investigate possible boundary signatures associated with boundary obstructed phases. For instance, the DMQI represents a BOTP with a filling anomaly. We can also easily build BOTPs with chiral or helical 1D hinge modes in 3D models, as we will show in Sec. IV. This means that, similar to bulk topological phases, we can have BOTPs associated with boundary states or filling anomalies. However, it is unlikely there are any boundary obstructions that are not associated with any boundary signatures. One intuitive way to understand this is by making a connection to the topology of the Wannier spectrum. If a topological distinction in the Wannier spectrum is only encoded in the exchange of a representation between the Wannier bands without any associated surface signature, then it is likely always possible to perform this exchange of representations by closing Wannier gaps *away* from the WCP (i.e., by exchanging representations with bulk states). In this case, a topological obstruction in the Wannier spectrum would not translate to an actual boundary obstruction. Per this discussion, we expect that there are no boundary obstructions that do not exhibit either boundary states or filling anomalies, but we leave a rigorous proof of such statement to future work. In the following, we will discuss some aspects of the boundary signatures of BOTPs in detail.

1. BOTPs with surface states

For boundary obstructions of this type, two phases are distinguished by the absence/existence of anomalous boundary states. In these cases, isolated groups of Wannier bands, at least in some directions, do not correspond to EBRs and cannot be associated with a spatial position. This is reflected in the fact that the *nested* Wannier spectrum shows spectral flow. If we restrict ourselves to electronic, charge-conserving systems where chiral or particle-hole symmetries are generally absent, this means that the only possible types of surface states are 1D helical (class AII) or chiral (class A) hinge states.

An example of the former is provided by the “dimerized

¹⁵ Here, we mean surface states which exhibit spectral flow which excludes zero-dimensional edge or corner states.

weak TI” [44], which can be constructed by stacking pairs of 2D quantum spin-Hall (QSH) insulators [3] with SSH-type coupling in the z -direction. In the presence of n -fold rotation symmetry C_{nz} and mirror symmetry M_z , this model fits into our definition of BOTP as explained in detail in Sec. IV C 2. By tuning the ratio of the inter- vs intra-cell coupling in the z -direction, we can induce transitions between two BOTPs distinguished by the existence of a dangling 2D QSH at the top and bottom surfaces, which hosts helical edge modes on hinges parallel to the x or y directions as shown in Fig. 19. Transitions between these two BOTPs require either closing the gap on the top and bottom surfaces (making the dangling 2D SPTs trivial), or on the side surfaces (making the SSH chains trivial so that we have paired SPT planes). The two BOTPs of the model can be interchanged if we add a 2D QSH at the top and bottom. However, the existence of a relative obstruction between them is a robust boundary feature that persists regardless of what is added at the boundary, and reflects the boundary obstruction between the two dimerizations. Similarly, we can construct BOTPs with chiral hinge modes by stacking Chern insulators with opposite Chern numbers with dimerized couplings along the stacking direction. This “dimerized weak Chern insulator” will be discussed in Sec. IV C.

2. BOTPs with filling anomalies

As discussed earlier, the DMQI provides the prototypical example of a BOTP with boundary obstructions associated with a filling anomaly. In this case, isolated groups of Wannier bands correspond to EBRs, and consequently atomic limits, which may be topologically distinct when the Wannier bands have residual symmetry. In the following, we will provide a discussion of filling anomalies associated with boundary obstructions in a more general setting. Recall that a filling anomaly is a condition that the system cannot be gapped, symmetric, and charge neutral at the same time. In the following, we will assume the first two conditions are always satisfied, and thus will identify filling anomalies with fractional charges in excess or deficit of neutrality. However, it should be noted that other ways to resolve the anomaly by preserving charge neutrality and breaking either the gap or the symmetry conditions are possible alternatives.

Let us start by considering a system with open boundary conditions that is invariant under a crystallographic point group G relative to a certain point in the bulk \mathcal{O} . If we consider any other point q , then its point group symmetry will satisfy $G_q \subseteq G$. The action of G on this point generates a set of symmetry-related points with $|G|/|G_q|$ elements; this set corresponds to a certain Wyckoff position \mathcal{Q} of the open system.

Let us now consider what happens when we close the boundaries by identifying edges to obtain a torus¹⁶. For a

point q on the boundary which is identified with a symmetry related point q' , the symmetry group is enlarged to $G_q^{(T)} \supset G_q$ (which still satisfies $G_q^{(T)} \subseteq G$). That is to say that the Wyckoff position \mathcal{Q} of the open system maps to a Wyckoff position of the periodic system with larger symmetry. As a result, the filling of q on the torus, $\nu_q^{(T)}$, is related to its filling in the open system ν_q by $\nu_q^{(T)} = \nu_q |G_q^{(T)}|/|G_q|$. From this relationship we can identify filling anomalies from the reverse procedure. That is, we start from a bulk/periodic, symmetric insulator and we are given the fillings of all the Wyckoff positions $\nu_q^{(T)}$. Then, if we open the boundaries there will be a filling anomaly associated to the position q if ν_q is fractional, i.e., if $\nu_q^{(T)}$ is not divisible by $|G_q^{(T)}|/|G_q|$. In words, the condition for a filling anomaly is that the filling of q in the open system must be fractional to preserve the symmetry at the filling fixed by the periodic symmetric insulator.

Next, let us investigate the conditions under which a filling anomaly does not imply a bulk obstruction. For example, we have already seen that the SSH chain has a filling anomaly and a bulk obstruction while the DMQI has a filling anomaly, but no bulk obstruction. Indeed, a bulk obstruction can be avoided if $\nu_q^{(T)}$ is large enough to allow us to symmetrically deform the electrons away from q . This is only possible if $\nu_q^{(T)}$ is a multiple of a certain number ν_q^{\min} which denotes the minimal filling of a point q on the torus at which it is possible to symmetrically deform the electrons away from q (and to the global center \mathcal{O}). Combined with the discussion above, we can now conclude that if we start with a periodic, symmetric insulator with fillings $\nu_q^{(T)}$, then a necessary condition for a BOTP filling anomaly is that for all q 's, $\nu_q^{(T)}$ is divisible by ν_q^{\min} , but for at least one q , $\nu_q^{(T)}$ is not divisible by $|G_q^{(T)}|/|G_q|$. As a consequence, boundary filling anomalies are impossible whenever ν_q^{\min} is a multiple of $|G_q^{(T)}|/|G_q|$ for all q . As we will see in later sections, this criteria will enable us to exclude the existence of simple 2D boundary obstructed models besides the DMQI, but will help us identify 3D BOTP models with filling anomalies.

D. Other 2D models

In this subsection, we investigate the possibility of boundary obstructions in other 2D systems apart from the DMQI. Following the discussion of the previous section, we will only focus on boundary obstructions associated with a boundary signature, i.e., surface states or filling anomalies. In a 2D system with gapped 1D edges, the only possible boundary states are zero-dimensional, and these require chiral or particle-hole symmetry for their protection [45]. For electronic insulators these symmetries can generically be broken, but the resulting systems will still be associated with a filling anomaly that

¹⁶ We assume here that the open system can be glued/identified into a torus

without singular points. We will discuss the possibility of more complicated open boundaries later.

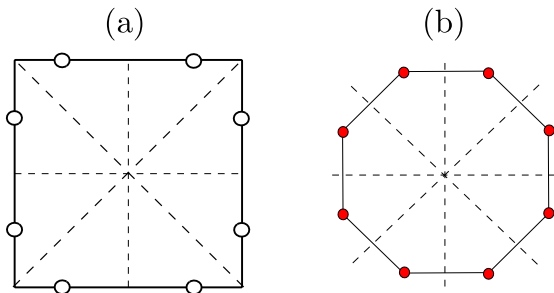


FIG. 11. (a) schematic illustration of a BOTP filling anomaly in the 2D point group D_4 associated with edge charges on a square geometry. (b) a more complicated edge termination which allows the localization of the zero modes to the corners (in the presence of an additional chiral symmetry) so that they can only be removed by closing the gap at a high-symmetry edge.

manifests as fractional boundary charges [25]. The boundary obstructions we seek, being deformable to the trivial atomic limit in the bulk, do not generate filling anomalies that scale with system length¹⁷. Thus, we will focus on only filling anomalies associated with 0D regions in this subsection.

Following the criteria of Sec. III C 2, we can easily find 2D systems, apart from the DMQI, with filling anomalies associated with boundary obstructions. For instance, consider the system with point group symmetry D_4 shown in Fig. 11a. The Wyckoff position consisting of a generic site q on the edge of the unit cell and its orbit under different symmetries is characterized by $|G_q^{(T)}| = 2$ (since it lies on a mirror line on the torus), $|G_q| = 1$, and $\nu_q^{\min} = 1$ (this corresponds to a filling of 4 per unit cell for the corresponding Wyckoff position Q). This means that when the filling of q on the torus is 1, it will be associated with a filling anomaly if the boundaries are opened such that q lies on the edges as shown in Fig. 11a.

There is, however, one problem with such an edge filling anomaly when considered on the standard square termination. To make this problem clear, let us consider this system in the presence of a chiral symmetry and a gap around zero energy modes localized at the corresponding Wyckoff position on the boundary. We note that the edges are high symmetry regions where approximate translational symmetry holds away from the corners. Assuming translation symmetry is unbroken just means that we cannot place the zero mode in the middle of an edge while maintaining the condition that the edge is gapped away from the zero mode. This means that the requirement of gapped edges would force the zero-modes to the corners where they annihilate. Hence, the existence of edge-localized modes is inconsistent with the existence of a gap at all high symmetry edges for the square termination. We can resolve this problem by choosing a more complicated ter-

mination shown in Fig. 11b, where the zero energy modes are localized on the 8 corners of an octagon. In this case, all edges are high symmetry regions, and the corner modes cannot be removed without closing the gap at some of the edges. However, we note that a such surface termination cannot be glued to form a torus without introducing some singular points; this is essentially a consequence of trying to maintain C_8 symmetry, a valid symmetry for an open geometry, when gluing the octagon to form a periodic lattice system, in which C_8 is not an allowed symmetry.

The previous example raises the questions of whether it is possible to find a BOTP in 2D apart from the DMQI where filling anomalies associated with corner states can be observed for a simple surface termination. Here, by ‘simple’ we mean that we require the surface termination to be identifiable into a torus without singularities, and the filling anomaly is associated with a *maximal* Wyckoff position, i.e., one which cannot be deformed to a more symmetric position, and as such will correspond to a corner state/charge rather than an edge state/charge. In the following, we will show that this is impossible.

To start the argument, consider a point q which is a part of a Wyckoff position Q on the torus and compare the size of its symmetry group on the torus $|G_q^{(T)}|$, with the size of the corresponding symmetry group on a system with open boundaries $|G_q|$. Now let us apply the criteria of Sec. III C 2. The possible symmetry groups that leave the point q invariant in 2D are the group of n -fold rotations C_n , or the n -fold dihedral group D_n , $n = 1, 2, 3, 4, 6$. Since we are focusing on filling anomalies associated with maximal Wyckoff positions, we exclude the trivial case C_1 , which represents general Wyckoff positions. In addition, we only consider points q with D_1 if the corresponding mirror line does not intersect any other mirror line, since otherwise q can be deformed to the more symmetric position at the intersection of the two mirror lines, and is therefore non-maximal. For point groups C_n or D_n , $n > 1$, the point q always corresponds to a maximal Wyckoff position.

Now, if the point group symmetry of q is C_n , then $\nu_q^{\min} = |G_q^{(T)}| = n$, which implies that a BOTP filling anomaly is impossible according to the criteria derived in Sec. III C 2. This is consistent with the observation that for the point group C_n , there is no surface termination with any high symmetry edges, i.e., edges with residual symmetry, implying the absence of edge obstructions, since edges without symmetry only allow for a trivial atomic limit.

If the point group symmetry of q is D_n , then the possibility of a BOTP filling anomaly depends on n . For $n = 1$ (when the mirror line does not intersect any other mirror line), $|G_q^{(T)}| = 2$ so a filling anomaly is only possible if the edge is chosen so that $|G_q| = 1$, i.e., the site symmetry group of q is reduced in the open system. In addition, the minimum filling to move the electrons away from q is $\nu_q^{\min} = 2 = |G_q^{(T)}|/|G_q|$ (from which the two electrons can move symmetrically away from the mirror line into the general Wyckoff position), which means that the filling anomaly is associated with a bulk rather than boundary obstruction (notice that this statement relies on

¹⁷ In bulk-obstructed phases, it is often the case that both edge-induced and corner-induced filling anomalies arise simultaneously, giving rise to gapless edges, and ill-defined corner charges if we require that neutrality is preserved.

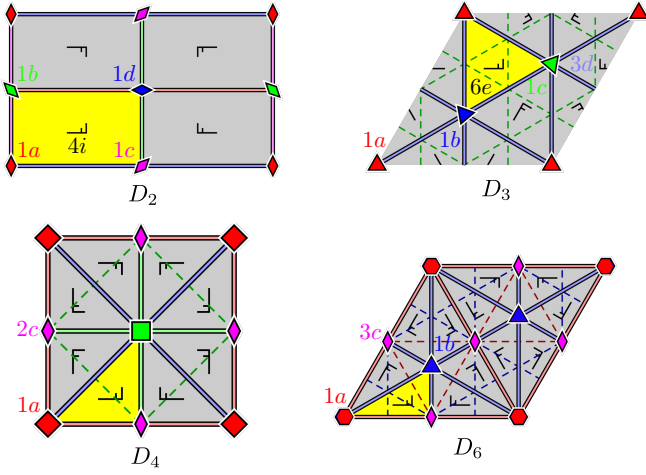


FIG. 12. Schematic illustration of the action of crystallographic point groups $D_{2,3,4,6}$ on the torus built by identifying opposite edges of a parallelogram (which is the same as the unit cell for the wallpaper group $D_n \times T^2$). The points with 2, 3, 4 and 6 fold symmetry are denoted by a diamond, triangle, square and hexagon, respectively. We can see from the figure that for $D_{3,4,6}$, all points with maximal symmetry are directly connected by mirror lines. The action of the crystallographic point groups $C_{2,3,4,6}$ are obtained from the above picture by removing the mirror lines (double stroke) and glide mirror lines (dashed stroke). The labels of the maximal Wyckoff positions are the same in C_n and D_n although their site symmetry group changes.

our requirement that q belongs to a maximal Wyckoff position such that it does not intersect with another mirror line).

The case $n = 2$ corresponds to a point q lying at the intersection of two mirror lines such that $|G_q^{(T)}| = 4$ and $\nu_q^{\min} = 2$. To obtain a filling anomaly on the open system, the boundary should be chosen such that q lies at an edge $|G_q| = 2$ or a corner $|G_q| = 1$. The former corresponds to $|G_q^{(T)}|/|G_q| = 2 = \nu_q^{\min}$ which is associated with a bulk filling anomaly, whereas the latter corresponds to $|G_q^{(T)}|/|G_q| = 4$ which does not divide ν_q^{\min} and corresponds to a BOTP filling anomaly. Thus, a BOTP filling anomaly is possible for point group D_2 at filling $\nu_q^{(T)} = 2$. This is realized by the DMQI discussed earlier.

For $n > 2$, $|G_q^{(T)}| = 2n$ and $\nu_q^{\min} = n$ since we can move n electrons away from a D_n -symmetric point along the mirror lines. This means that a BOTP filling anomaly is possible if $|G_q| = 1$. This is however impossible for any symmetric edge termination¹⁸ since all points with maximal D_n symmetry on the torus are connected by mirror lines for $n > 2$ as shown in Fig. 12, so that their symmetry group in the open system contains at least two elements. This implies that regardless of which point we choose to be the central high symmetry point \mathcal{O} in the open system, all other points with D_n symmetry on

the torus will lie on mirror lines, thus corresponding to points with $|G_q| = 2$ in the open system.

Thus, the only 2D crystallographic point group which allows for BOTPs on symmetric open boundaries that can be glued into a non-singular torus is D_2 . We note that lifting the requirement that the point group is crystallographic, or equivalently that the boundary can be identified into a torus, makes it possible to find other 2D BOTPs. Since boundary terminations that can be glued to form periodic crystal lattices are simpler to handle, and can be analyzed in momentum space using Wannier spectra, we will focus on such types of boundaries in what follows. We leave the detailed study of other 2D BOTPs to future works and move on to a proposal for new 3D BOTPs.

IV. 3D MODELS WITH BOUNDARY OBSTRUCTIONS

A. Recipe for constructing 3D BOTPs

We now switch our attention to BOTPs in 3D. In the following, we present a simple recipe that can be used to construct 3D models with different types of boundary obstructions. The recipe works in analogy to the construction of the 2D DMQI model. For that model, we took a pair of inversion symmetric SSH chains along, say the x -direction, in each unit cell and then coupled them with dimerized couplings, i.e., intra- and inter-cell couplings γ_y and λ_y along the y -direction (i.e., the stacking direction). Additionally, to generate the necessary symmetry structure, we threaded a π -flux per unit cell (Fig. 1). In the limit $\gamma_y = 0$, $\lambda_y \neq 0$, there is an isolated/unpaired SSH chain on each of the edges parallel to the x -axis that can be in the trivial ($|\gamma_x| > |\lambda_x|$) or obstructed ($|\gamma_x| < |\lambda_x|$) atomic limit, and thus may have an associated boundary obstruction.

This construction suggests a route to obtaining 3D BOTPs: we start with any 2D Hamiltonian $\mathcal{H}_{2D}(\mathbf{k})$ associated with boundary signatures such as corner/edge charges or 1D edge states. We then consider a pair of these Hamiltonians such that their sum is topologically trivial and all the associated boundary signatures can be removed when they are coupled. Next, we couple these pairs via dimerized SSH-like couplings γ_z, λ_z along the (stacking) z -direction. This arrangement guarantees that in the limit $\gamma_z = 0$, $\lambda_z \neq 0$, there is a single isolated copy of $\pm\mathcal{H}_{2D}(\mathbf{k})$ at the upper/lower surface when the system is considered with open boundaries. Additionally, to ensure that the bulk gap is open if either $\mathcal{H}_{2D}(\mathbf{k})$ is gapped or $|\gamma_z| \neq |\lambda_z|$, we insert π fluxes between the stacked layers (i.e., in the xz and yz plaquette types). The resulting 3D Hamiltonian is given by

$$\mathcal{H}_{3D}(\mathbf{k}) = \mathcal{H}_{2D}(\mathbf{k})\tau_3 + \lambda_z\tau_2 \sin k_z + (\gamma_z + \lambda_z \cos k_z)\tau_1, \quad (8)$$

where $\tau_{1,2,3}$ denote the Pauli matrices in the layer subspace along z . Due to the π fluxes, the different terms of the Hamiltonian anticommute which implies that it can only be gapless if each of the three terms separately vanish, i.e. only if $\mathcal{H}_{2D}(\mathbf{k})$ is gapless and $|\lambda_z| = |\gamma_z|$.

¹⁸ A symmetric edge termination is one that preserves the symmetry D_n relative to some global origin \mathcal{O} .

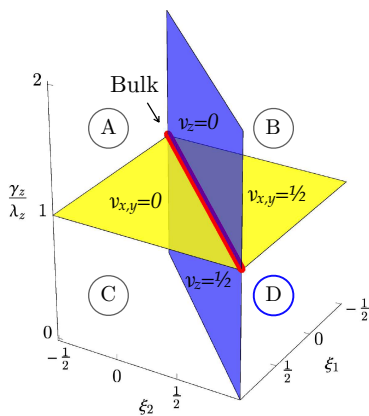


FIG. 13. Generic phase diagram for $\mathcal{H}_{3D}(\mathbf{k})$ obtained by the three dimensional construction in Sec. IV A, where the two dimensional Hamiltonian $\mathcal{H}_{2D}(\mathbf{k})$ is parameterized by $\{\xi_1, \xi_2\}$. As an illustration we choose the 2D model to exhibit two topologically distinct phases depending on which of ξ_1 or ξ_2 is the largest. Hence, $\mathcal{H}_{2D}(\mathbf{k})$ has a bulk gap closing transition at $\xi_1 = \xi_2$ that will subsequently lead to a Wannier gap closing in $\mathcal{H}_{3D}(\mathbf{k})$ in the \mathcal{W}^z Wannier spectrum (blue plane), which can happen at $\nu_z = 0$ or $\nu_z = 1/2$ as labeled in the figure. On the other hand, the gap in the \mathcal{W}^x and \mathcal{W}^y Wannier spectra closes when the stacks of $\mathcal{H}_{2D}(\mathbf{k})$ are uniformly coupled in the stacking direction, i.e., when $\lambda_z = \gamma_z$ (yellow plane), again either at $\nu_{x,y} = 0$ or $\nu_{x,y} = 1/2$ as labeled in the figure. The intersection between the two planes corresponds to a line where the bulk gap is closed in the phase diagram. This construction yields four phases A, B, C and D separated by Wannier gap closings. A choice of boundary may select one of the four to be topologically distinct from the other three (in the sense of a boundary obstruction) when the Wannier gap closing happens at the Wannier chemical potential. Here we highlighted phase D as a non-trivial boundary obstructed topological phase for a choice of boundary termination that coincides with the unit cell structure, $\mu_i = 1/2$.

The type of boundary obstruction in the 3D Hamiltonian (8) depends on the type of obstruction for $\mathcal{H}_{2D}(\mathbf{k})$ as well as the dimension of its surface states. For the top/bottom surfaces, $\mathcal{H}_{3D}(\mathbf{k})$ will have a surface (hinge) obstruction if $\mathcal{H}_{2D}(\mathbf{k})$ has a bulk (edge) obstruction. For side surfaces, $\mathcal{H}_{3D}(\mathbf{k})$ will have a surface (hinge) obstruction if $\mathcal{H}_{2D}(\mathbf{k})$ has hinge states/charges (corner charges). The latter statement can be understood by investigating the dimension of the SPT needed to add to the side surfaces to cancel the surface states/charges (remember all BOTPs are extrinsic HOTIs whose surface states can be removed by adding a lower dimensional SPT on the surface). If the 2D Hamiltonian has corner charges, then it is enough to add 1D SSH chains to the vertical hinges to cancel them. On the other hand, a 2D Hamiltonian with hinge states or charges requires the addition of a 2D SPT on the side surfaces to cancel these states/charges. It follows from the previous discussion that $\mathcal{H}_{3D}(\mathbf{k})$ has a surface (hinge) obstruction if and only if $\mathcal{H}_{2D}(\mathbf{k})$ has a bulk (edge) obstruction with 1D (0D) edge states/charges. We note that it is also possible to have mixed surface-hinge obstructions where connecting two BOTPs involves either a surface gap-

closing on the upper/lower surfaces or a hinge gap-closing on the side surfaces. This would be the case if, for example, we take $\mathcal{H}_{2D}(\mathbf{k})$ to be a bulk-obstructed atomic insulator with corner charge e.g. the C_4 quadrupole model. It is worth noting that the distinction between surface and hinge types of obstructions is only possible for boundaries consisting of several intersecting 2D planes. On a more smooth boundary like a sphere, such a distinction is ill-defined.

A representative phase diagram of the above construction can be found in Fig. 13. There we consider a two dimensional Hamiltonian parametrized by generic parameters ξ_1 and ξ_2 . For illustration we assume the 2D Hamiltonian admits topologically nontrivial phase with boundary modes if $\xi_1 > \xi_2$, a trivial phase when $\xi_1 < \xi_2$ and a critical point when $\xi_1 = \xi_2$. When stacking into a three dimensional system, the bulk 3D Hamiltonian will be gapped even when $\xi_1 = \xi_2$ as long as there is a dimerization along z , $\lambda_z \neq \gamma_z$. As a function of ξ_1, ξ_2 , and γ_z/λ_z there is a line in the phase diagram (red line) where the bulk is gapless. By construction, this model allows for four adiabatically connected bulk phases, separated by Wannier gap transitions where the Wannier spectra changes its topology. A choice of a symmetric boundary termination will single out one of the phases, where the Wannier gap closing happens at the WCP, (for our choice this is at $\nu_{x,y} = 1/2$ and $\nu_z = 1/2$) (c.f. Fig. 13). For this boundary termination, which coincides with the unit cell structure, phase D is a non-trivial boundary obstructed topological phase since $\lambda_z > \gamma_z$ leaving a dangling $\mathcal{H}_{2D}(\mathbf{k})$ on the top and bottom surfaces that is in its topologically nontrivial phase.

In the following two subsections, we will focus on models with surface obstructions while briefly discussing an example of a hinge obstruction. We will separately consider the cases where the surface obstruction is associated with a filling anomaly or anomalous boundary states.

B. 3D BOTPs with filling anomalies

In this subsection, we will discuss 3D BOTPs associated with filling anomalies leading to fractional hinge or corner charges. We will propose a class of models with C_{2nh} symmetry $n = 1, 2, 3$ exhibiting surface obstructions associated with a hinge charge. After introducing the models, we analyze their properties using a real-space approach as well as through the Wannier spectrum. At the end, we will briefly discuss an example of a hinge-obstructed model with corner charge.

1. A new class of C_{2nh} Hamiltonians

Now, let us introduce a new class of 3D models defined for the crystallographic point groups C_{2nh} with $n = 1, 2, 3$, that have *surface* obstructions associated with *hinge* charges. These symmetry groups are characterized by a $2n$ -fold rotation C_{2nz} accompanied by a mirror reflection perpendicular to the rotation axis M_z . The filling anomalies in these models do not occur for points q where $G_q = G$, but instead at positions

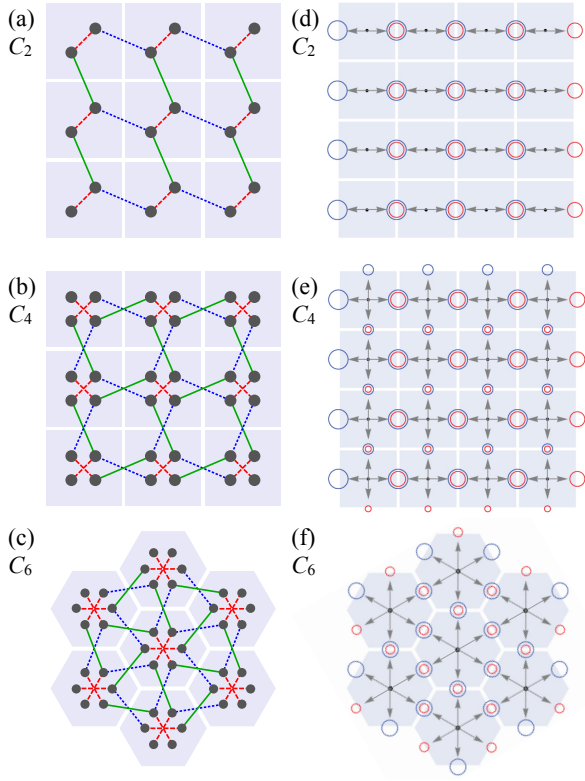


FIG. 14. (a,b,c) Schematic illustration of the 2D hopping Hamiltonians used to build the 3D quadrupole models with (a) C_2 , (b) C_4 , and (c) C_6 symmetries. The hopping parameters λ_0 , λ_x and λ_y are denoted by red, green, and blue lines respectively. (d,e,f) Top view illustration of the deformation process explained in the text between position $1a$ and position $1c$ for (d) C_2 , (e) C_4 , and (f) C_6 symmetries.

where $G_q = C_{2h} \subset G$.¹⁹

We build the 3D Hamiltonians in each case following the recipe of Sec. IV A using 2D models that realize a C_{2n} insulator at filling n . The full 3D model will be a 3D BOTP at filling of $2n$. The 2D tightbinding Hamiltonians we use are shown in Fig. 14. Each of these 2D models has several distinct atomic limit phases separated by a bulk transition: one where all the $2n$ electrons are at the center of the unit cell (with site symmetry group C_{2n} , c.f. Fig.12 red \mathcal{Q}); and others where the $2n$ electrons are distributed in pairs to n symmetry related edges of the unit cell (with site symmetry C_2 , c.f. Fig.12 purple \mathcal{Q}). The non-trivial obstructed atomic limit of these models is characterized by edge charges so they can be understood as weak 2D phases if translation symmetry in the 2D plane is preserved.

Explicitly, the C_2 model is given by

$$\mathcal{H}_{2D}^{C_2}(\mathbf{k}) = (\lambda_x \sin k_x + \lambda_y \sin k_y) \sigma_2 + (\lambda_0 + \lambda_x \cos k_x + \lambda_y \cos k_y) \sigma_1, \quad (9)$$

where $\sigma_{1,2,3}$ denote the Pauli matrices distinguishing the two atomic orbitals inside the unit cell. The hopping parameters $\lambda_{0,x,y}$ are represented by the black, green, and blue links in Fig. 14a, respectively. The spectrum of Eq.(9) is given by

$$\varepsilon^2 = \lambda^2 + 2\lambda_0(\lambda_x \cos k_x + \lambda_y \cos k_y) + 2\lambda_x \lambda_y \cos(k_x - k_y), \quad (10)$$

with the shorthand $\lambda^2 = \lambda_0^2 + \lambda_x^2 + \lambda_y^2$. The 2D model is gapped whenever the largest of $\lambda_{0,x,y}$ exceeds the sum of the other two. In addition, the gapped phases at half filling correspond to distinct atomic insulators with a single electron localized either at the $1a$, $1b$, or $1c$ positions (cf. Fig 12) whenever the largest λ is λ_0 , λ_x , or λ_y , respectively.

The 2D Hamiltonians for C_4 and C_6 symmetric cases can be constructed in a straightforward way. We simply stack two or three copies of $\mathcal{H}_{2D}^{C_2}(\mathbf{k})$ related by C_4 or C_6 rotations, respectively. They are shown schematically in Fig. 14b,c. Let us here explicitly show the resulting C_4 model, by adding to the C_2 model a $\pi/2$ rotated copy of itself,

$$\mathcal{H}_{2D}^{C_4}(\mathbf{k}) = \begin{pmatrix} \mathcal{H}_{2D}^{C_2}(\mathbf{k}) & 0 \\ 0 & e^{i\frac{\pi}{4}\sigma_1} \mathcal{H}_{2D}^{C_2}(c_4\mathbf{k}) e^{-i\frac{\pi}{4}\sigma_1} \end{pmatrix}, \quad (11)$$

where $c_4\mathbf{k} = (k_y, -k_x)$ is the real space action of C_4 . This Hamiltonian describes a 2D four-band model.

Following the recipe in Sec. IV A, let us take a pair of C_2 models and stack them with dimerized couplings γ_z , λ_z along the z -direction. Additionally, we thread a π -flux per unit cell in the xz and yz plaquettes. This causes the C_2 and M_z symmetries to anticommute. As we will explain later, the anti-commutation of the two spatial operations allows for the filled electrons to occupy a continuously movable \mathcal{Q} , which is necessary in our construction of BOTPs (see also Sec. II B). The resulting 3D Hamiltonian with point group C_{2h} is given by Eq. (8), and it satisfies the symmetry relations

$$M_z \mathcal{H}(\mathbf{k}) M_z^\dagger = \mathcal{H}(m_z \mathbf{k}), \quad M_z = \sigma_3 \tau_1 \\ C_2 \mathcal{H}(\mathbf{k}) C_2^\dagger = \mathcal{H}(c_2 \mathbf{k}), \quad C_2 = \sigma_1 \tau_0, \quad (12)$$

where $m_z \mathbf{k} = (k_x, k_y, -k_z)$ and $c_2 \mathbf{k} = (-k_x, -k_y, k_z)$. The eight-band C_{4h} model has the symmetries

$$C_4 = e^{-i\frac{\pi}{4}} \begin{pmatrix} 0 & e^{i\frac{\pi}{4}\sigma_1} \\ e^{i\frac{\pi}{4}\sigma_1} & 0 \end{pmatrix} \tau_0, \quad M_z = \begin{pmatrix} \sigma_3 & 0 \\ 0 & \sigma_2 \end{pmatrix} \tau_1. \quad (13)$$

Here $\sigma_{1,2,3}$ act in the space of orbitals within the same 2D layer, whereas $\tau_{1,2,3}$ act in the space of orbitals in different layers. The C_6 model has a similar structure.

2. Real space picture and filling anomaly

We now explain the boundary obstruction in the models described in the previous subsection. Similar to the discussion of the DMQI in Sec. II B, we consider the real-space defor-

¹⁹ We notice that in discussing the symmetry group of a certain Wyckoff position, we focus only on the spatial part. Other extra internal symmetries may exist, particularly in the presence of the π fluxes, that extend the point group, for example, by the element $\bar{1}$ as in the DMQI.

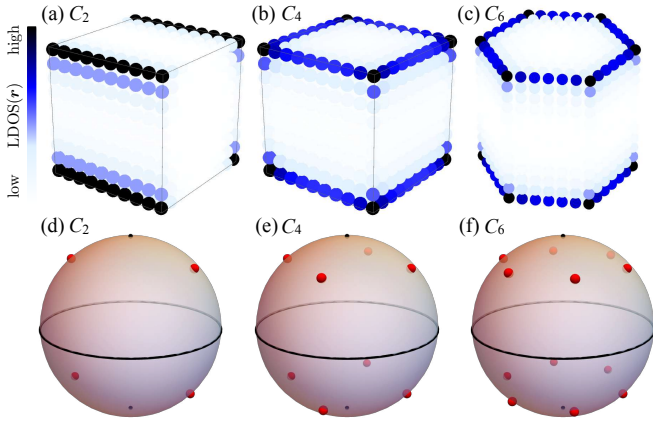


FIG. 15. (a,b,c) local density of states at zero energy for the surface obstructed insulators constructed by stacking the tight binding models from Fig. 14 with (a) C_2 , (b) C_4 , or (c) C_6 symmetry. We can clearly notice the existence of hinge-localized states associated with hinge charges if we require the system to be symmetric and gapped, or alternatively a partially filled hinge band if we require the system to be symmetric and neutral; both phenomena are a result of the filling anomaly. (d,e,f): illustration of the 0D surface states associated with the filling anomaly for a spherical surface termination. Such states can only be annihilated at the high symmetry regions at the equator or north/south poles leading to a gap-closing at these points.

mation between two distinct configurations of the electrons: one where all electrons are at the center of the unit cell $1a$ (cf. Fig.12, red \mathcal{Q}) at the $z = 0$ plane, and the other with two electrons at the edge of the unit cell $1c$, $2c$ or $3c$ (nc for shorthand) in the three different models (cf. Fig.12, purple \mathcal{Q}) at the $z = 1/2$ plane. This can be done while preserving the symmetry by first moving the $2n$ electrons at $1a$ horizontally in the $z = 0$ plane into nc as shown in Fig. 14; and then moving the 2 electrons at this site vertically in opposite directions. We could also start by first moving n electrons vertically in each direction, then moving them horizontally to position nc . However, we note that the first trajectory (which involves moving horizontally then vertically) will be obstructed in the presence of side surfaces at the unit cell edge. The reason is that at such side surfaces, the filling of the nc position is 1, and thus we cannot further move the electrons vertically while preserving the mirror symmetry in the z direction. Similarly, the second trajectory involving vertical then horizontal movement is not possible in the presence of the top/bottom surfaces at the $z = 1/2$ plane. The reason is that the filling of the position $1a$ at this surface is n (rather than $2n$ which is its bulk filling). This does not allow us to symmetrically move the electrons in the plane to position nc without breaking the symmetry.

This discussion parallels the one of Sec. II B for the DMQI, and it shows that in the presence of a surface termination consistent with the unit cell shown in Fig. 14, it is not possible to connect the atomic configuration where the $2n$ electrons are at $1a$ in the $z = 0$ plane to the one where 2 electrons are at position nc at the $z = 1/2$ plane, despite the fact that these two atomic configurations are symmetrically deformable to each

other in the bulk (with periodic boundaries). We also note that, similar to the DMQI case, the possibility of interpolating the two atomic configurations in the bulk imposes some constraints on the commutation properties of the different symmetries, i.e.,

$$\{C_2, M_z\} = 0. \quad (14)$$

In Appendix B we provide a real-space argument for this relation.

Let us now discuss the boundary signature for the C_{2nh} models which, as we will see, has the form of a hinge filling anomaly. To show this, we recall that the discussion of Sec. III C 2 where the existence of a filling anomaly is based on the filling of a position q on the torus $\nu_q^{(T)}$ not being divisible by the ratio of the order of its site symmetry group on the torus and in the open system $|G_q^{(T)}|/|G_q|$. For all the C_{2nh} models discussed above, the bulk filling for the nc position at $z = 1/2$ in the obstructed phase is $\nu_q^{(T)} = 2$, and its symmetry group on the torus is $G_q^{(T)} = C_{2h}$ (generated by C_{2z} and M_z) which has four elements, $|G_q^{(T)}| = 4$. For the surface termination where the vertical surfaces are at the edges of the unit cell (shown in Fig. 14a,b,c), and the horizontal surfaces are at $z = 1/2$, the sites q lying at the horizontal hinges (see Fig. 15a,b,c) have no symmetry left. Thus $|G_q| = 1$ for these points, and this implies a fractional filling of $1/2$ per unit cell.²⁰ Notice here that we assumed approximate translational symmetry along the hinges such that we can define a charge per unit cell. The hinge-localized states associated with hinge charges are shown in Fig. 15a,b,c, for the three C_{2nh} models for $n = 1, 2, 3$. As mentioned earlier, we always assume our systems are gapped everywhere, and that the symmetry is unbroken, so that a filling anomaly implies the existence of fractional charges in excess or deficit of neutrality. If we instead preserve symmetry and charge neutrality we find instead that the hinges are partially filled bands, and are thus gapless in these models.

It is worth pointing out that the filling anomaly will also manifest itself even for surfaces without any approximate translational symmetry at the surface, e.g., a sphere. In this case, we can understand the filling anomaly by first imposing chiral symmetry and noting that we can associate the anomaly with $2n$ 0D surface states at generic symmetry related points on the surface as shown in Fig. 15d,e,f. Such 0D states can only be annihilated at the equator or the north/south poles where a gap-closing indicates a boundary phase transition since they are high symmetry regions. Following the discussion of Sec. II D, the filling anomaly will survive even after breaking chiral symmetry.

²⁰ We note that sites lying on the vertical or horizontal surfaces also have no symmetry left relative to the origin of the open system \mathcal{O} . However, these sites may have approximate symmetries associated with the approximate translational symmetry along these surfaces. This is not the case for the hinges which do not have any spatial symmetries left.

3. Wannier spectrum

We now turn our attention to the evolution of the Wannier bands and how they encode the boundary obstructions described in the previous subsection. We diagnose the boundary obstruction by analyzing the Wannier spectrum and choosing a lattice termination that coincides with the edges of the unit cell. That is, the WCP is given by $(\mu_x, \mu_y, \mu_z) = (1/2, 1/2, 1/2)$, which means that only gap closings of the Wannier spectrum at these values correspond to actual boundary gap closings. A phase diagram of the models is shown for reference in Fig. 16.

C_{2h} model— A gapped Wannier spectrum along \hat{z} is possible provided $\mathcal{H}_{2D}^{C_2}$ is in a gapped phase. This only happens when $2\lambda_M > \lambda_S$ (blue regions in Fig. 16), where we defined the parameters $\lambda_S = \lambda_x + \lambda_y + \lambda_0$ and $\lambda_M = \max(\lambda_x, \lambda_y, \lambda_0)$. On the other hand, the Wannier spectrum along \hat{x} or \hat{y} is gapped as long as $|\gamma_z| \neq |\lambda_z|$ (yellow plane in Fig. 16). The bulk Hamiltonian is gapped if either condition is satisfied, and is therefore only gapless in the intersections of the blue region and yellow plane in the phase diagram. The region of intersection is marked in red. It is evident that the Wannier gap may close while preserving the bulk gap, a necessary condition for a BOTP. We show the Wannier spectra $\nu_z(k_x, k_y)$ and $\nu_x(k_z, k_y)$ in Figs. 17a and 18a. In these figures, we can see six distinct regions with gapped Wannier spectra separated by Wannier gap closings, as will be explained in detail below.

Similar to the DMQI case, the different gapped phases of the C_{2h} model are characterized by distinct Wannier band representations, which can be reflected in distinct values of the nested Wannier band polarizations. Let us first notice that the model has four quantized Wannier band polarizations: $p_{z,x}$ and $p_{z,y}$ are quantized due to C_2 symmetry, and $p_{x,z}$ and $p_{y,z}$ are quantized by M_z symmetry. In our model, $p_{z,x}$ and $p_{z,y}$ cannot be simultaneously non-zero, and $p_{x,z}$ and $p_{y,z}$ are equal, leading to six distinct gapped phases (see Fig. 16). Let us label the different phases by the maximal Wyckoff position \mathcal{Q} around which the Wannier centers are located, as shown in Fig. 16b. While the electrons may be symmetrically displaced from this maximal Wyckoff position in some cases, they remain centered around \mathcal{Q} , and both their band representations, and Wannier band representations, are topologically equivalent to those of the phase where the electrons lie exactly at \mathcal{Q} . Therefore it is useful to label the phases by such maximal Wyckoff positions. We can use the notation $(p_{z,x}, p_{z,y}, p_{x,z}, p_{y,z})_{\mathcal{Q}}$, to label the six distinct phases, which are given by: $(0, 0, 0, 0)_{1a}$, $(0, 1/2, 0, 0)_{1b}$, $(1/2, 0, 0, 0)_{1d}$, $(0, 0, 1/2, 1/2)_{1c}$, $(0, 1/2, 1/2, 1/2)_{1g}$, $(1/2, 0, 1/2, 1/2)_{1f}$. In our model we cannot tune parameters such that the Wannier centers lie at the $1e$ or $1h$ Wyckoff positions.

The Wannier transitions between the different phases can be studied numerically leading to the phase diagram in Fig. 16a. As we can see, all the mutual Wannier transitions between the phases $1a$, $1b$, and $1d$ are associated with a gap-closing of the Wannier spectrum in the z -direction at $\nu_z = 0$. On the other hand, the mutual Wannier transitions between the phases $1c$, $1g$, and $1f$ are associated with a gap-closing for the Wannier

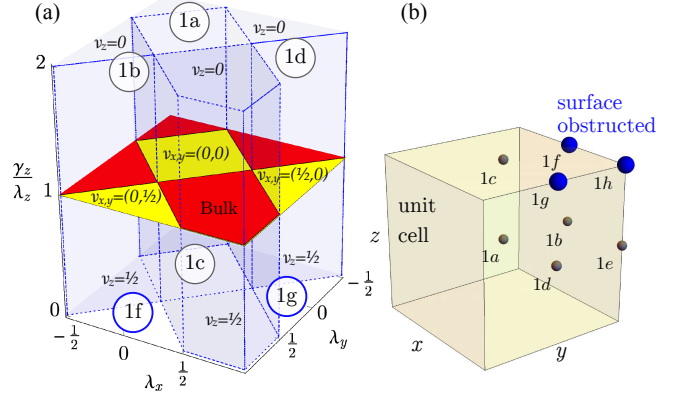


FIG. 16. (a) Phase diagram for the C_{2h} model introduced in Sec. IV B 1 with a fixed value of $\lambda_0 = 1/2$. The Wannier spectrum \mathcal{W}^z closes at the blue regions which span the γ_z/λ_z axis in the areas marked with \mathcal{W}^z ; while the Wannier spectrum \mathcal{W}^x closes at the yellow plane at $\gamma_z/\lambda_z = 1$. Due to the constraints in the model, a gap closing in \mathcal{W}^x implies a gap closing in \mathcal{W}^y . In the intersection between the two, the red regions, the bulk is gapless. The gapped phases with gapped Wannier spectra are marked by the representative maximal \mathcal{Q} from which the Wannier band representations may be induced. (b) Spatial location of the maximal \mathcal{Q} 's compatible with the C_{2h} point group. With the conventional choice of Wannier chemical potential $(1/2, 1/2, 1/2)$, phases induced from $1f$, $1g$, and $1h$ may be surface obstructed; from $1h$ they could also be hinge obstructed. In our model we realize $1f$ and $1g$ surface obstructions.

spectrum in the z -direction but at $\nu_z = 1/2$. This reflects the fact that transitions between $1a$, $1b$, and $1d$ take place in the $z = 0$ plane, whereas transitions between $1c$, $1f$, and $1g$ take place in the $z = 1/2$ plane. The Wannier transitions $1a \leftrightarrow 1c$, $1b \leftrightarrow 1f$ and $1g \leftrightarrow 1d$ are associated with a gap-closing in both Wannier spectra along the x and y directions occurring at $(\nu_x, \nu_y) = (0, 0)$, $(0, 1/2)$, and $(1/2, 0)$, respectively.

Following the previous discussion, we can see that the phases $1f$ and $1g$ have a surface obstruction, which can be diagnosed by $p_{x,z} = p_{y,z} = 1/2$ and $(p_{z,x}, p_{z,y}) = (0, 1/2)$ or $(1/2, 0)$, respectively. They are characterized by a quantized hinge charge of $1/2$ per unit cell, at the hinges along \hat{y} or \hat{x} respectively. A real space calculation of the low energy states is found in Fig. 15a,b,c. As an example, in Figs. 17 and 18 we show how the two gapped phases, $1a$ and $1g$, which correspond to the parameters $(\lambda_0, \lambda_x, \lambda_y, \gamma_z, \lambda_z) = (0.5, 0, 0.25, 0.5, 1)$ and $(\lambda_0, \lambda_x, \lambda_y, \gamma_z, \lambda_z) = (0.5, 1, 0.25, 1.5, 1)$ respectively, are separated by a Wannier gap closing transition at the WCP, and consequently a surface gap closing. We follow two distinct paths, either by first increasing $\lambda_x : 0 \rightarrow 1$, and then increasing $\gamma_z : 0.5 \rightarrow 1.5$, or vice versa. When increasing λ_x first, the gap at the $z = 1/2$ surface closes in the range of $0.25 \leq \lambda_x \leq 0.75$, (c.f. gapless $\nu_z(k_x, k_y)$ in Fig. 17 a2 and a3). Instead, if we increase γ_z first we find the gap closing at the WCP at $\gamma_z = 1$, (c.f. gapless $\nu_x(k_y, k_z)$ in Fig. 18 b). Thus, a surface gap-closing at the $z = 1/2$ or $x = 1/2$ surface is unavoidable whenever we connect the $1a$ and $1g$ phases.

Finally, we comment on the Wannier band representations.

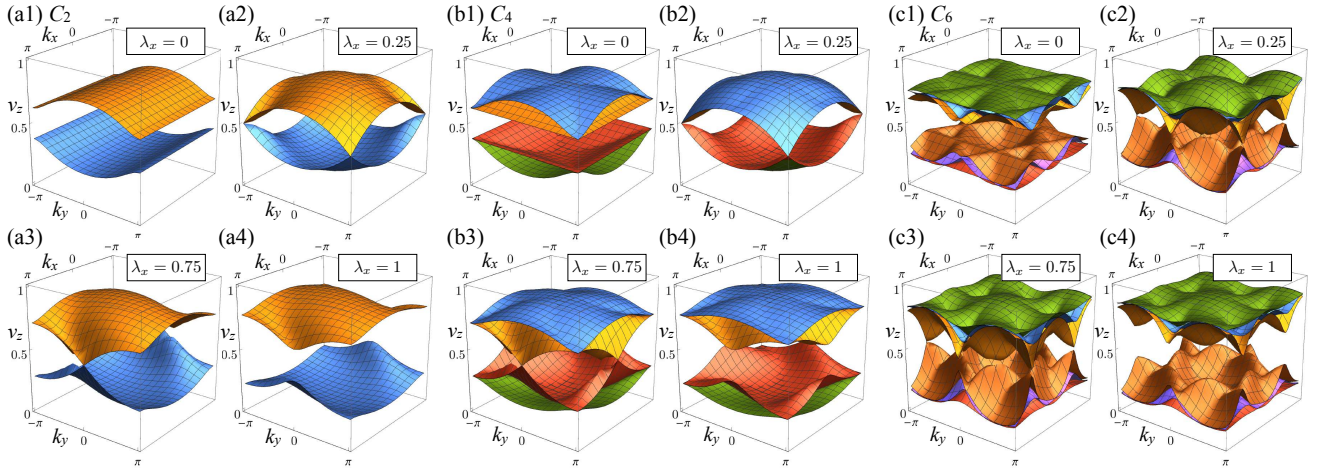


FIG. 17. Evolution of the Wannier spectrum \mathcal{W}^z with eigenvalues $\nu_z(k_x, k_y)$ for different values of λ_x in the three-dimensional boundary obstructed models with filling anomalies and C_{2h} , C_{4h} and C_{6h} symmetries. The other parameters are kept fixed at the values of $\lambda_0 = .5$ and $\lambda_y = .25$ with $\lambda_z = 1.5$ and $\gamma_z = 1$. With gapped ν_x (see text), we find that varying λ_x allows for two gapped phases bordered by an extended region where ν_z is gapless. This happens when $.25 < \lambda_x < .75$ where the condition $2 \max(\lambda_0, \lambda_x, \lambda_y) < (\lambda_0 + \lambda_x + \lambda_y)$ is satisfied. Panels (a1) and (a4) correspond to the gapped phases $1f$ and $1g$ in the phase diagram of Fig.16, respectively.

\mathcal{Q}	$w_1^{z,\Gamma}(C_2)$	$w_1^{z,\mathbf{X}}$	$w_1^{z,\mathbf{Y}}$	$w_1^{z,\mathbf{M}}$	$w_1^{x,\Gamma}(M_z)$	$w_1^{x,\mathbf{Z}}$
1a	+	+	+	+	+	+
1b	+	+	-	-	+	+
1c	+	+	+	+	+	-
1d	+	-	+	-	+	+
1f	+	+	-	-	+	-
1g	+	-	+	-	+	-
1e	+	-	-	+	+	+
1h	+	-	-	+	+	-
×	+	+	+	-	+	+
×	+	+	+	-	+	-

TABLE I. Upper section of rows: Diagnosis of boundary obstructions through Wannier band representations in the C_{2h} model the model introduced in Sec. IV B 1. The left column indicates the maximal Wyckoff position \mathcal{Q} that labels the phase with periodic boundaries. In the columns to the right we show the symmetry representations at high symmetry momenta of one of the two WBRs. They are evaluated for C_2 and M_z according to which symmetry is preserved in the respective direction. Middle section of rows: Other possible WBR configurations compatible with the C_{2h} point group, but not realized by our model. Bottom section of rows: Example of Wannier symmetry indicators that are not WBRs. These may correspond to boundary obstructed phases with anomalous surface states, where the Wannier bands in \mathcal{W}^z are characterized by a Chern number. Examples of these type of obstructions are discussed in Sec.IV C. We leave the value of \mathcal{Q} blank since a Chern number precludes these phases from being associated with a Wyckoff position. Throughout the table, the bold lines correspond to the phases with a boundary obstruction when the conventional Wannier chemical potential is chosen, i.e., $(\mu_x, \mu_y, \mu_z) = (1/2, 1/2, 1/2)$.

The Wannier spectrum of \mathcal{W}^z , corresponds to the upper and lower surfaces (which preserve C_2), while the Wannier spectrum of $\mathcal{W}_{x/y}$ correspond to the side surfaces (which preserves M_z). The WBRs corresponding to $w^{z,\mathbf{k}}$ and $w^{x/y,\mathbf{k}}$

are split into two disconnected WBRs when $2\lambda_M > \lambda_S$ or $|\gamma_z| \neq |\lambda_z|$, respectively. The values that the WBRs take at high symmetry momenta \mathbf{K} may be used to determine the topological phases. To determine these symmetry indicators we induce the bulk BR's from the maximal \mathcal{Q} 's and subduce them to the subgroup maintained by the respective Wannier spectrum, as described in Sec.III B. The resulting symmetry indicators are explicitly shown in Table I. As anticipated earlier, we can see that the C_2 eigenvalues for $1a/1c$, $1b/1f$, and $1d/1g$ correspond to a 2D inversion symmetric insulator with a single electron localized at $(0, 0)$, $(0, 1/2)$, and $(1/2, 0)$, respectively. Similarly, The M_z eigenvalues correspond to a 2D mirror-symmetric system where the electron is localized at the 0 or $1/2$ mirror lines for $1a/1b/1d$ or $1c/1f/1g$, respectively.

C_{4h} model— We now look at the 8 band model with C_{4h} symmetry. The model differs from the C_{2h} model in two main aspects. First, C_4 symmetry dictates that the Wannier spectra \mathcal{W}^x and \mathcal{W}^y are identical, hence the nested polarizations $p_{z,x}$ and $p_{z,y}$ are equal. This means the model has only *one* non-trivial phase, and this phase has hinge charge along both the x and y directed hinges. In this phase, the occupied electrons are distributed around the $1f$ and $1g$ positions in Fig. 16b. Second, with four occupied electrons per unit cell, the Wannier bands allow for more complicated gap-closing patterns, as we will see below.

The analysis of the C_{4h} model parallels the one for the C_{2h} model above. The model has four distinct regions of gapped Wannier spectra characterized by the values of the two distinct nested polarizations $(p_{z,x}, p_{x,z})$ equal to $(0, 0)_{1a1a}$, $(0, 1/2)_{1c1c}$, $(1/2, 0)_{1b1d}$, and $(1/2, 1/2)_{1f1g}$, and separated by Wannier gap-closings. The transitions $1a1a \leftrightarrow 1c1c$ and $1b1d \leftrightarrow 1f1g$ are characterized by Wannier gap-closings at $\nu_x = \nu_y = 0$ and $\nu_x = \nu_y = 1/2$, respectively, whereas the transitions $1a1a \leftrightarrow 1b1d$ and $1c1c \leftrightarrow 1f1g$ are characterized by Wannier gap-closings at $\nu_z = 0$ and $\nu_z = 1/2$,

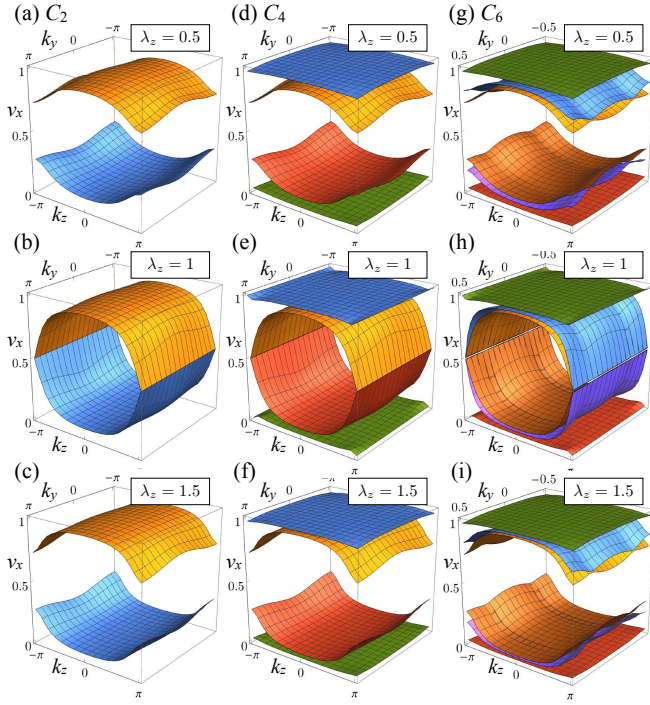


FIG. 18. Evolution of the Wannier spectrum \mathcal{W}^x with eigenvalues $\nu_x(k_y, k_z)$ for different values of λ_z and fixed $\lambda_0 = .5$, $\lambda_x = 1$, $\lambda_y = .25$, and $\lambda_z = 1$. Across these that ν_x is gapped, we find the gapless transition of ν_x to happen when $\lambda_z = 1$. Panels (a) and (c) correspond to the gapped phases $1g$ and $1d$ in the phase diagram of Fig. 16, respectively.

respectively. As a result, the $1b1d$ phase is a BOTP that cannot be reached from any of the three other phases without closing a gap at the boundary for our chosen boundary termination (corresponding to a WCP $\mu_{x,y,z} = 1/2$).

This can be seen more directly by studying the evolution of the Wannier bands. The Wannier bands in the z -direction calculated via \mathcal{W}^z are shown in Fig. 17b. The four bands are split into two groups of two bands. Akin to the C_{2h} model, when $\lambda_M = \lambda_0 > \lambda_S/2$, the two filled bands are located around $1a$ with $p_{z,x} = p_{z,y} = 0$. On the other hand, when $\lambda_M = \lambda_{x,y} > \lambda_S/2$, the two filled bands describe one electron at $1f$ and one at $1g$, each having $p_{z,x} = p_{z,y} = 1/2$. In both cases, the Wannier bands form an EBR and cannot be split further. In particular, this implies that the Wannier gap closing when $\lambda_M < \lambda_S/2$ involves all four bands.

Focusing on \mathcal{W}^x , we can similarly investigate the transition between the two distinct phases by tuning γ_z . Here, we find a gap closing transition when $|\gamma_z| = |\lambda_z|$ (c.f., Fig. 18). Unlike \mathcal{W}^z , the bands are split into four separate bands (four EBRs) since the symmetries of \mathcal{W}^x do not relate them. This follows from the fact that, with only mirror symmetry, all non-general Wyckoff positions have multiplicity 1. This implies that all EBRs that are not derived from the general position are one-dimensional. As a result, the gap closing at the WCP takes place only between two of the four Wannier bands. This implies that we can identify the different phases by looking at the (nested) Wannier band polarization of a single band. The

phase with hinge charge is characterized by $p_{x,z} = 1/2$.

C_{6h} model—We can define a model with C_{6h} symmetry in a very similar fashion. The 2D Hamiltonian used to construct this model (via Eq. (8)) is schematically illustrated in the third panel of Fig. 14. The behavior of the model is qualitatively similar to the models above. Namely, there are two phases distinguished by a surface obstruction as shown in Figs. 17c and 18c. The non-trivial phase is characterized by a fractional hinge charge per unit cell (c.f. Fig. 15c).

4. A hinge-obstructed 3D BOTP

One of the simplest 3D BOTPs we can construct is a trivial dimensional extension of the DMQI. Following the recipe of Sec. IV A, we can create a 3D BOTP by stacking pairs of DMQI's. Since the DMQI is edge-obstructed and has corner charges, the resulting 3D BOTP has a hinge obstruction associated with a filling anomaly which translates to a corner charge of $e/2$ at each of the 8 corners.

The filling anomaly can be understood by noting that the 3D model has mirror symmetries about three perpendicular planes, i.e., M_x, M_y , and M_z . When considered on a torus, i.e., with periodic boundary conditions, then there are 8 points q with maximal symmetry $|G_q^{(T)}| = 8$, where the three perpendicular mirror planes intersect. These points correspond to the 8 maximal Wyckoff positions of multiplicity 1. Whenever the filling of such points is a multiple of two, we can symmetrically move the electrons along the intersection of any two of the three mirror planes to reach any of the other symmetric positions. On the other hand, with open boundaries, the site q that lies on a corner of the open system has its site symmetry group reduced such that $|G_q| = 1$. At a bulk filling of $\nu_q^{(T)} = 4$ (which is natural for a pair of DMQI's), the sites at the corners will have a filling of $1/2$ signaling the existence of a BOTP filling anomaly. Such a filling anomaly is associated with a hinge rather than surface obstruction. Indeed, this model is exactly the octupole insulator of Refs. 15 and 16, which was the first example of a 3D BOTP. Due to being hinge-obstructed, its boundary obstruction is encoded in the band representations of the nested Wannier bands rather than the WBR themselves.

C. 3D BOTPs with anomalous surface states

In the previous section, we discussed models with boundary obstructions associated with filling anomalies. Here, we construct two models with anomalous boundary states due to a surface obstruction: the dimerized weak Chern insulator and the dimerized weak TI. Both of these models are constructed using the recipe of Sec. IV A.

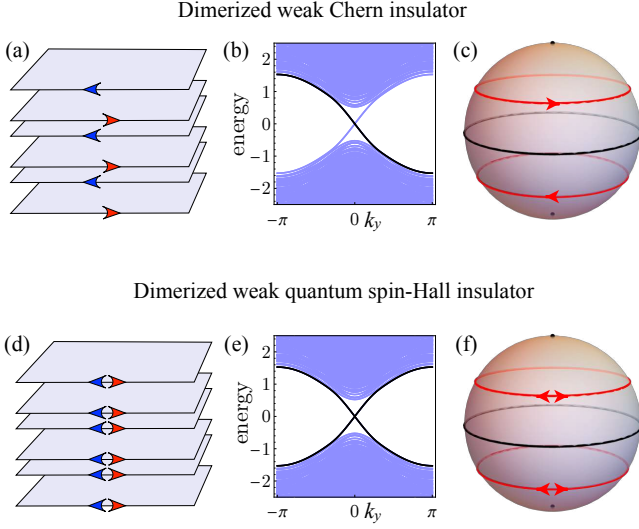


FIG. 19. Three dimensional boundary obstructed phases without a Wannier representation: dimerized weak Chern insulator protected by $M_z\mathcal{T}$ and C_{2z} (top panel), and the dimerized weak Topological insulator protected by both M_z , \mathcal{T} , and C_{2z} (bottom panel). Left: Scheme of the model where the arrows indicate chiral one-dimensional modes that can be gapped by a coupling along z . In the two nontrivial cases, either a 2D Chern insulator or a 2D topological insulator is left unpaired at the surface. Center: Energy spectrum of a system with translation symmetry along y but finite along both x and z . The ingap states are located at the top and bottom hinges. We have marked in black the band that is exponentially localized at one hinge. Right: illustration of the 1D surface states on a spherical surface termination. The equator and north/south pole are invariant under M_z and C_{2z} , respectively. The 1D surface states can only be symmetrically removed by closing the gaps at one of these high symmetry regions.

1. Dimerized weak Chern insulator

In the first model we consider a stack of pairs of Chern insulators with opposite Chern number related by a combination of time-reversal symmetry and M_z symmetry. The pairs are coupled with a dimerized SSH coupling along the z -direction and there is π -flux threaded in the xz and yz plaquettes. In addition, we also assume the presence of two-fold rotation around the z -axis C_{2z} . The 3D Hamiltonian is given by (8) where

$$\mathcal{H}_{2D}(\mathbf{k}) = \sin k_x \sigma_1 + \sin k_y \sigma_2 + (2 + m - \cos k_x - \cos k_y) \sigma_3. \quad (15)$$

\mathcal{H}_{2D} has a Chern number of 0 for $|2+m| > 2$ and $\text{sgn}(2+m)$ for $|2+m| < 2$. Let us assume in the following discussion that $|m| < 2$ so that the Chern number is just determined by the sign of m . The 3D Hamiltonian is invariant under the product $M_z\mathcal{T} = \sigma_1\tau_1\mathcal{K}$, with \mathcal{K} denoting complex conjugation, as well as $C_{2z} = \sigma_3$. With open boundaries coinciding with the boundary of the unit cell, the model hosts two dangling 2D Chern insulators with opposite Chern numbers at the top and

bottom layers when $|\gamma_z| < |\lambda_z|$. Changing the sign of m induces a gap closing in the top and bottom surfaces, signaled by a closing the Wannier gap along the z -direction (c.f. Fig. 20a). If, on the other hand, m is kept negative, and γ_z is tuned through a point where $|\gamma_z| = |\lambda_z|$, the Wannier gaps along the x and y directions close (c.f. Fig. 20b). This model exhibits a boundary obstruction separating the gapped phase with parameters ($|\gamma_z| > |\lambda_z|, m < 0$) from ($|\gamma_z| < |\lambda_z|, m \leq 0$) and ($|\gamma_z| \leq |\lambda_z|, m > 0$).

An interesting aspect of this model is that the Wannier obstruction for \mathcal{W}^z has a different origin from \mathcal{W}^x and \mathcal{W}^y . In the Wannier spectrum of \mathcal{W}^z , the obstruction is associated with a non-zero Chern number, i.e., the Wannier bands do not separately form WBRs, as illustrated by the non-trivial spectral flow of the *nested* Wannier spectrum as shown in Fig. 21a and e. On the other hand, the Wannier obstruction in \mathcal{W}^x or \mathcal{W}^y is associated with changes in the nested Wannier band polarization between values of 0 and $1/2$ as shown in Fig. 21c, d, g, and h. There we can see that the average value of p is either 0 or $1/2$. These distinct values are evidence that the Wannier bands in Fig. 20d and f are distinct WBRs, characterized by different eigenvalues of M_z at high symmetry momenta (c.f. Table I, bottom row).

It is important to highlight the role played by the C_{2z} symmetry here. Although it is not needed as a traditional protecting symmetry for the Wannier topology, it is crucial to single out the upper and lower surfaces as high symmetry planes where Wannier gap-closings imply a surface phase transition. Similar to the discussion of Sec. III A, this can be illustrated by considering a spherical geometry as shown in Fig. 19c. Under $M_z\mathcal{T}$ alone, only the equator is a high symmetry region, and we are generally allowed to smoothly deform the chiral hinge modes by shrinking them to a point without touching the equator. In the presence of C_{2z} , however, the north and south poles become HSPs where surface gap-closings indicate a surface phase transition per our definition. Note that allowing for distinctions captured by gap-closings at generic, non-HSPs will generate the same spurious, uncountable boundary distinctions as those discussed in Sec. III A. We also note that C_{2z} symmetry is convenient in diagnosing the boundary obstruction in terms of symmetry eigenvalues for the WBRs. The configuration of C_2 eigenvalues for a nontrivial Wannier band is shown in Table I.

2. Dimerized weak quantum spin Hall insulator

Similar to the dimerized weak Chern insulator, the dimerized weak quantum spin Hall insulator is constructed by stacking 2D quantum spin Hall (QSH) insulators with a dimerized coupling along \hat{z} (with π -fluxes inserted in the xz and yz plaquettes). A minimal Hamiltonian for the QSH insulator is provided by the four-band model [3]

$$\mathcal{H}_{2D}(\mathbf{k}) = \sin k_x \sigma_1 \mu_0 + \sin k_y \sigma_2 \mu_0 + (2 + m - \cos k_x - \cos k_y) \sigma_3 \mu_2. \quad (16)$$

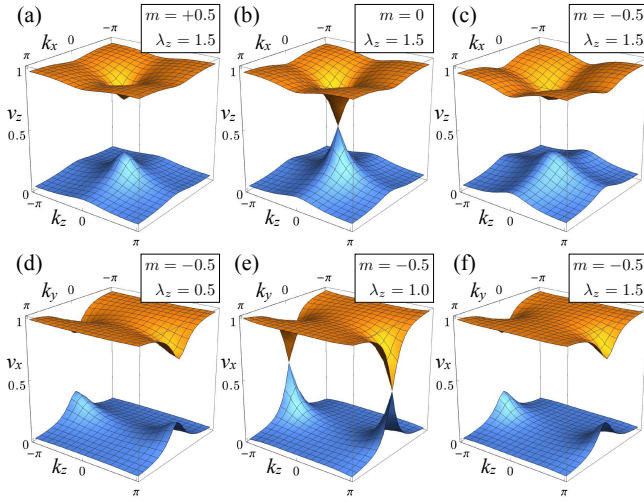


FIG. 20. Evolution of the \mathcal{W}^z (a-c) and \mathcal{W}^x (d-f) Wannier spectra of the dimerized weak Chern insulator model for different values of m and λ_z with fixed $\gamma_z = 1$. Entering the phase with $m = -0.5$ and $\lambda_z = 1.5$ requires a Wannier gap closing at $\nu = 1/2$ both when tuning m or λ_z . This phase is therefore separated by a boundary phase transition for a boundary with the conventional Wannier chemical potential $\mu_{x,y,z} = 1/2$.

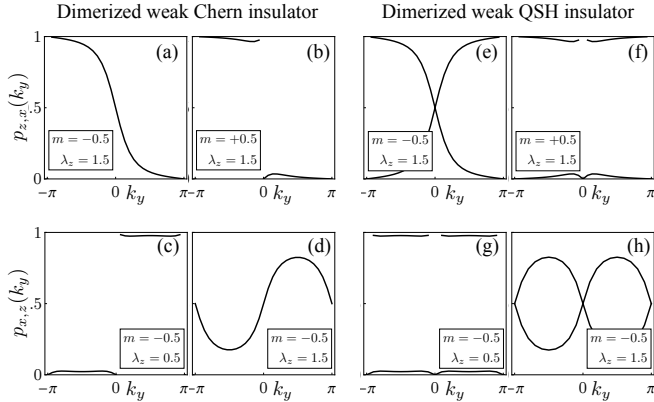


FIG. 21. Nested polarization $p_{z,x}(k_y)$ and $p_{x,z}(k_y)$ for different values of m and λ_z with fixed $\gamma_z = 1$ in the dimerized weak Chern insulator (a-d) and weak quantum spin-Hall insulator (e-h). The phase with $m = -0.5$ and $\lambda_z = 1.5$ (a,e) is characterized by a winding of the nested polarization which indicates that the Wannier bands in \mathcal{W}^z do not form band representations and are associated with hinge modes. On the other hand, $p_{x,z}(k_y)$ is gapped with a different average value in the two phases, either 0 (c,g) or $1/2$ (d,h), reflecting the fact that \mathcal{W}^x decomposes into distinct Wannier band representations.

Here, σ and μ denote the Pauli matrices in the spin and orbital spaces respectively. The Hamiltonian is invariant under the spinful time-reversal symmetry $\mathcal{T} = i\sigma_2\mathcal{K}$ and $C_{2z} = \sigma_3$. Again, we obtain the 3D Hamiltonian from Eq. (8), and this results in a Hamiltonian with an extra mirror symmetry given by $M_z = \sigma_3\mu_3\tau_1$. The Wannier spectra of the model are very similar to the weak Chern insulator since this model is just two time-reversed copies of the Chern insulator model. Thus, we

see a Wannier transition at the WCP in \mathcal{W}^z when $|\lambda_z| > |\gamma_z|$, and $m = 0$; as well as a Wannier transition at the WCP in \mathcal{W}^x and \mathcal{W}^y when $m < 0$ but $|\gamma_z| = |\lambda_z|$. However, in contrast to the dimerized weak Chern insulator, this model has four filled bands. Each of the Wannier bands is two-fold degenerate at time-reversal invariant momenta, and the additional C_2 symmetry causes this degeneracy to appear across the entire surface Brillouin zone.

The nested Wannier spectra of this model are shown in Fig. 21. We note that $\nu_{z,x}(k_y)$ resembles that of the spectral flow in a quantum spin Hall insulator. Two Wannier bands flow in opposite directions, crossing at $k_y = 0$ and π where the degeneracy cannot be lifted due to Kramers' theorem. This nested Wannier winding captures the dangling QSH at the upper and lower surfaces. On the other hand, $\nu_{x,z}(k_y)$ in the nontrivial phase shows two bands related by time-reversal symmetry, each with average polarization of $1/2$. Although the total polarization vanishes, the polarization for each component of the Kramers' pair does not, and it is such a quantized (time-reversal) polarization [46] that captures the Wannier transition in $\nu_x(k_y, k_z)$. In general one could use a description of the time-reversal polarization in terms of a Pfaffian invariant[46] but we will not pursue that further here. In this case the Wannier transition resembles the transition in a spinful SSH chain with time-reversal and inversion symmetry where the edge anomaly is associated with Kramers' pairs of electrons rather than an individual electron.

In summary, both the dimerized weak Chern model and the dimerized weak quantum spin-Hall model exhibit one-dimensional propagating hinge states that can be removed without closing the bulk gap. However, removing the hinge states requires closing the energy gap at for at least one high-symmetry surface. These systems only admit a Wannier representation for periodic boundaries but not for open boundaries. This serves to illustrate that boundary obstructions are not restricted to Wannier representable systems.

V. DISCUSSION

In this work, we introduced the notion of boundary topological obstructions that captures topological obstructions which do not exist on periodic boundaries, but exist on geometries with symmetric open boundaries. In more precise terms, we call two Hamiltonians \mathcal{H}_1 and \mathcal{H}_2 boundary-obstructed if they can be symmetrically deformed to each other without closing the gap for periodic boundary conditions, but not for open boundary conditions which preserve the symmetries. Another way to formulate this is by saying that any symmetric deformation of \mathcal{H}_1 to \mathcal{H}_2 involves a gap-closing at a high-symmetry region on the *boundary* rather than the *bulk*, as in the case of conventional SPTs. We stress that our definition of boundary obstructions captures a bulk property, and excludes the cases where a non-trivial lower-dimensional SPT is attached at the boundary of a trivial bulk system.

One important subtlety in defining boundary obstructions is the requirement that the boundary choice is fixed throughout the deformation process such that the two Hamiltonians

are compared *with the same boundary*. This, in turn, relies on the existence of a canonical way to choose open boundary terminations that is independent of the bulk Hamiltonian. There are several ways to do this, and here we chose the termination procedure described by Eq. 5, and inspired by Ref. [37]. Such a choice has the advantage of connecting the boundary spectrum to easily computable bulk quantities such as the Wannier and entanglement spectra. The topological obstructions studied in this work are all associated with robust boundary signatures such as surface states or filling anomalies, thus we believe them to be independent of the chosen way to implement the boundary termination. We emphasize that, although BOTPs can be trivialized by adding some SPTs on the boundary, the *relative* distinctions between them is stable provided that the boundary is fixed throughout the deformation process. This is similar to the relative distinction that exists in the 1D SSH chain with quantized charge polarization.

For most of this work, we focused on boundary obstructions in d -dimensional system that are associated with a gap-closing at a $(d - 1)$ -dimensional surface hyperplane, i.e., an edge obstruction in 2D, or a surface obstruction in 3D. Such obstructions can be analyzed by investigating the Wannier spectrum for the Wilson loop operator in the direction perpendicular to the surface hyperplane. We also employed the formalism of band representations developed in Refs. [29, 35, 36] to show how a bulk BR decomposes into a set of Wannier band representations separated by Wannier gaps. Importantly, BRs that are equivalent in the bulk can decompose into different WBRs that cannot be deformed to each other without closing one of the Wannier gaps. This defines a notion of topological distinctions in the Wannier spectrum. To relate this to surface obstructions, a surface termination is chosen. Such a choice picks one particular Wannier gap (marked by a Wannier chemical potential) to be the one corresponding to the actual surface gap. Surface obstructed topological phases are then defined as equivalence classes of bulk BRs which are equivalent as bulk BRs, but correspond to distinct WBRs that cannot be deformed to each other without closing the Wannier gap at the WCP for some surface.

In Sec. II, we used the double-mirror quadrupole insulator (DMQI) of Ref. [15, 16] as a prototypical example to illustrate the notion of BOTPs. Although this model has been intensively studied as one of the first examples of a HOTI, one crucial aspect of it had so far been overlooked. Namely, the fact that in the absence of C_4 symmetry, the two ‘phases’ of the model are not SPTs in the standard sense since they can be deformed to each without closing the bulk gap in periodic boundary conditions. Using the notion of BOTP, we provide a resolution to this problem by showing that such ‘phases’ are related by a boundary rather than bulk obstruction. This was investigated in detail from several different perspectives including real space orbital deformations, Wannier spectra, and symmetry representations. The latter was particularly useful in establishing the connection between the boundary obstruction in the model and the existence of a filling anomaly. Indeed the existence of a filling anomaly allows for a topological boundary signature that does not rely on the existence of zero-energy corner states (which, for insula-

tors, typically require fine-tuned symmetries such as particle-hole or chiral symmetry). Instead, it reflects the fact that the model, when filled with electrons to neutrality, cannot be simultaneously gapped, symmetric and charge-neutral. Thus, a symmetric, gapped DMQI at half-filling will necessarily have excess/deficit charge of $2e$ equally distributed among the four corners yielding a fractional corner charge of $e/2$.

In Sec. IV, we introduced several 3D models for BOTPs. The first family of such BOTPs have similar phenomenology to the DMQI and exhibit surface obstructions. The non-trivial BOTPs in this family are associated with filling anomalies similar to the one in the DMQI, and they manifest in fractional hinge charge (per unit cell) when the system is symmetric and gapped at half-filling. In addition, we introduced a second family of BOTPs characterized with chiral/helical propagating hinge modes. In both cases, the existence of a boundary obstruction is established explicitly by studying the Wannier spectra and the symmetry indicators of the corresponding WBRs.

Before closing, let us discuss the possible extension of the concepts discussed here beyond free fermions. We note that the existence of chiral/helical hinge states or filling anomalies are robust features that are expected to survive in the presence of interactions. Thus, we expect the boundary topological distinctions we found here to still be relevant for interacting systems. On the other hand, defining boundary obstructions is likely more tricky for interacting phases since it requires the implementation of a surface termination in a canonical way which does not depend on the bulk phase. It is unclear whether this is generally possible which makes it difficult to decide what it means to “keep the boundary fixed,” or to compare two phases with the “same boundary.” We leave the investigation of such questions to future works.

Finally, it is worth stressing that, unlike SPTs, the surface theories for BOTPs are not anomalous, i.e., they can be realized as an independent lower dimensional system without breaking any symmetry. However, the fact that their properties are generated by the bulk introduces some subtleties compared to stand-alone lower dimensional systems. These include the fact that the topological properties of different surfaces are not completely independent (since they derive from the same bulk), and that some topological obstructions can be evaded by coupling to the bulk degrees of freedom (cf. Sec. III C).

ACKNOWLEDGMENTS

We thank Barry Bradlyn, Jennifer Cano, Dominic Else, Adrian Po, Ryan Thorngren, and Ashvin Vishwanath for stimulating discussions. E. K. was supported by a Simons Investigator Fellowship, by NSF-DMR 1411343, and by the German National Academy of Sciences Leopoldina through grant LPDS 2018-02 Leopoldina fellowship. W. A. B. thanks the support of the Eberly Postdoctoral Fellowship at the Pennsylvania State University. T. L. H. thanks US National Science Foundation (NSF) grants EFMA-1627184 (EFRI), and DMR-1351895 (CAREER) for support. R. Q. was funded by the

Deutsche Forschungsgemeinschaft (DFG, German Research Foundation) Projektnummer 277101999 TRR 183 (project B03), the Israel Science Foundation, and the European Research Council (Project LEGOTOP).

Author Contributions: E. K. developed the general definition for boundary obstructions, the general correspondence between Wannier and boundary topology, proposed 3D model examples, aided the development of the real-space, band representation, and filling anomaly approaches to BOTPs, and was the primary manuscript writer. W. A. B. developed the connection between real-space Wannier center deformation and boundary obstructions, helped develop the Wannier band representation, real-space, and filling anomaly approaches to BOTPs, and helped in the writing of the manuscript. T. L. H. contributed to the refinement of all of the conceptual advances of the paper and helped in the writing of the manuscript. R. Q. developed the formalism of band representation theory of BOTPs, helped develop the real-space and Wannier spectrum approaches to BOTPs, developed the filling anomaly arguments in BOTPs, helped in the writing of the manuscript, and led the initiation of the collaboration.

Appendix A: Character table of D_2^π

Rep. / class	$\{1\}$	$\{\bar{1}\}$	$\{M_x M_y\}$	$\{M_y\}$	$\{M_x\}$
A_1	1	1	1	1	1
A_2	1	1	1	-1	-1
B_1	1	1	-1	1	-1
B_2	1	1	-1	-1	1
\bar{E}	2	-2	0	0	0

TABLE II. Character table of the point group D_2^π defined in the main text.

Appendix B: Real Space Proof of Anti-commuting Symmetries

1. Anticommuting Mirrors in the 2D DMQI

We now show that in order to carry out the deformation between the configurations at $1a$ and $1d$ in the DMQI, it is necessary that the two mirror operators anticommute. This is suggested by the fact that the two configurations actually correspond to *different* symmetry representations for commuting mirrors, but the same symmetry representation for anticommuting mirrors (\bar{E}). We will see that the anticommuting mirrors can be inferred from the real space picture in Fig. 3. Let us start with the orbitals at position $1a$ and then move them horizontally using position $2e$ into position $1c$. The two orbitals in position $2e$ are related by mirror symmetry M_x and have the form $|(\pm x, 0)\rangle$, where $|\mathbf{r}\rangle$ denotes an orbital localized at point \mathbf{r} . In this basis, M_x is off-diagonal and acts generally as $M_x |(\pm x, 0)\rangle = e^{\pm i\phi} |(\mp x, 0)\rangle$ (with some arbitrary phase ϕ), leading to the eigenvectors $|(+x, 0)\rangle \pm e^{i\phi} |(-x, 0)\rangle$ whose eigenvalues are ± 1 respectively. Since these orbitals lie

on the $y = 0$ mirror line, they are eigenvectors of M_y . Next, to bring these orbitals to position $1d$, we move them vertically using position $2h$. In this position, the action of M_y is off-diagonal, thus, following the same argument as for M_x , we can deduce that it has two distinct eigenvalues $+1$ and -1 . Since the symmetry eigenvalues cannot change under smooth, symmetry-preserving deformations, we deduce that $M_y = \pm \sigma_3$ in the $2e$ basis. In the same basis, we showed that $M_x = \sigma_1 \exp\{i\phi\sigma_3\}$, which in turn implies $\{M_x, M_y\} = 0$. Since anticommutation is basis-independent, we deduce that connecting the $1a$ and $1d$ positions at a filling of two electrons per cell requires M_x and M_y to anticommute. We note that the connection of mirror anticommutation in the DMQI model to important quadrupole properties was proposed in Refs. [15, 16] based on a study of the Wannier spectrum.

2. Anticommuting C_2 and M_z for 3D C_{2nh} Models

To show that C_2 and M_z anticommute for the C_{2nh} models that we discuss in Section IV B 1, we note that in order to occupy a movable Wyckoff position that interpolates between $1a$ and nc in the M_z invariant planes, the Wannier centers permute into each other under the action of C_{2n} . This implies the eigenvalues of the C_{2n} operator must span all the $2n$ roots of unity $e^{\pi i l/n}$ with $l = 0, \dots, 2n - 1$. Similarly, to occupy a vertically movable Wyckoff position at C_2 invariant lines, the eigenvalues of M_z should be ± 1 since its action is a permutation of the two sites in this position. Noting that the two electrons at position nc originate from electrons which have moved away from the center $1a$ in diametrically opposite directions, and are thus related by C_2 , we find that the requirement of deformability in the vertical direction forces any pair of C_2 -related orbitals to have opposite mirror eigenvalues. Thus, in a basis where the mirror symmetry M_z is diagonal, C_2 is purely off-diagonal and it switches the positive and negative mirror sectors which implies the anticommutation condition

$$C_2 M_z C_2^\dagger = -M_z. \quad (\text{B1})$$

This discussion is very similar to the one for the DMQI above.

Appendix C: Band representations and movable Wyckoff positions

We now review the construction of a band representations (BRs) following Refs.[29, 36]. We consider an orthogonal set of localized Wannier states $|\mathbf{R}; q_\alpha, i\rangle$ where \mathbf{R} is a Bravais lattice vector, with a spatial dependence

$$\langle \mathbf{r} | \mathbf{R}; q_\alpha, i \rangle = W_{\alpha, i}(\mathbf{r} - \mathbf{R}) \quad (\text{C1})$$

centered at q_α . A state at q_1 transforms under the representation Λ_{q_1} of the site symmetry group $G_q \subseteq G$, where G is the full symmetry group, and we omit the subscript on q because the G_q are isomorphic for each q_α . The transformation of the

Wannier orbitals is

$$g|\mathbf{R}; q_1, i\rangle = \Lambda_{q_1}(g)_{ij} |\mathbf{R}; q_1, j\rangle, \quad (\text{C2})$$

for $g \in G_q$. The index i runs through the dimension of the representation Λ_{q_1} which from now on we omit, adopting a vector notion of $|\mathbf{R}; q_\alpha\rangle$. The sum over repeated indices is also implicit. The action of additional lattice symmetries that do not leave q_1 invariant may be found under the action of the elements of the coset G/G_q , leading to the formation of a Wyckoff position \mathcal{Q} , whose different sites are labelled by $\alpha = 1, \dots, N_{\mathcal{Q}}$ where $N_{\mathcal{Q}}$ is the multiplicity of the Wyckoff position. Since the action of G/G_q on the Wyckoff position \mathcal{Q} is free and transitive, we can define g_α as the group element that satisfies $g_\alpha |\mathbf{R}; q_1\rangle = |\mathbf{R}; q_\alpha\rangle$. Hence, we can write the representation of the full Wyckoff position \mathcal{Q} induced from the representation at q_1 as $\Lambda_{\mathcal{Q}} = \Lambda_{q_1} \uparrow G$ of the point group G^{21} ,

$$g|\mathbf{R}; q_\alpha\rangle = \Lambda_{\mathcal{Q}}(g)_{\alpha\beta} |g\mathbf{R}; q_\beta\rangle \equiv \Lambda_{q_1}(g_\beta^{-1}gg_\alpha) |g\mathbf{R}; q_\beta\rangle, \quad (\text{C3})$$

for any element $g \in G$. This point group representation $\Lambda_{\mathcal{Q}}$ is used in the main text to label the states. In the DMQI with open boundaries the G representation is $\Lambda_{2a} = \bar{E}$ at high symmetry lines and $\Lambda_{4c} = E \otimes \bar{E}$ for the general Wyckoff position.

Adding translations to form the (symmorphic) space symmetry group $G^{(T)} = G \times T^d$, we can choose a basis where the point group operations act on a single unit cell, because we can translate the transformed states back into the original unit cell with $T_{\alpha\beta}$,

$$g|\mathbf{R}; q_\alpha\rangle = \Lambda_{q_1}(g_\beta^{-1}T_{\beta\alpha}^{-1}gg_\alpha) |g\mathbf{R} + \mathbf{R}_{\beta\alpha}; q_\beta\rangle, \quad (\text{C4})$$

where $\mathbf{R}_{\beta\alpha} = gq_\alpha - q_\beta$ is the lattice vector that connects the two sites. Having lattice translation symmetry it is natural to write the representation of the symmetry group $G^{(T)}$ as a function of crystal momentum. This can be done by first Fourier transforming the Wannier states into Bloch states $|\mathbf{k}; q_\alpha\rangle = \sum_{\mu} \exp\{i\mathbf{k} \cdot \mathbf{R}\} |\mathbf{R}; q_\alpha\rangle$. The Hamiltonian in this basis is given by,

$$\mathcal{H}(\mathbf{k}) = E_{\alpha,i}(\mathbf{k}) |\mathbf{k}; q_\alpha, i\rangle \langle \mathbf{k}; q_\alpha, i|, \quad (\text{C5})$$

where $E_{\alpha,i}(\mathbf{k})$ are the band energies. The BR induced from the G_q representation Λ_{q_1} ,

$$g|\mathbf{k}; q_\alpha\rangle = \rho_{\Lambda_{\mathcal{Q}}}^{\mathbf{k}}(g)_{\beta\alpha} |g\mathbf{k}; q_\beta\rangle, \quad (\text{C6})$$

can be computed explicitly from

$$\rho_{\Lambda_{\mathcal{Q}}}^{\mathbf{k}}(g)_{\beta\alpha} = \exp\{-ig\mathbf{k} \cdot \mathbf{R}_{\beta\alpha}\} \Lambda_{\mathcal{Q}}(g_\beta^{-1}T_{\beta\alpha}^{-1}gg_\alpha), \quad (\text{C7})$$

and fully describes the symmetry content and the momentum space Berry-Zak phases of the bands of the Hamiltonian \mathcal{H} .

Two representations ρ and $\tilde{\rho}$ are equivalent if and only if there is a unitary and smooth matrix-valued function $S(t, g)$ respecting $S(0, g) = \rho(g)$ and $S(1, g) = \tilde{\rho}(g)$ for all symmetry group elements g . In a crystalline system, the unitary matrix that generates these changes $S(t, g) = U(t - t', g)^\dagger S(t', g) U(t - t', g)$, continuously implements a basis transformation of ρ . As discussed in Ref. [47], when ρ is an induced representation from a point q into G , and $\tilde{\rho}$ is an induced representation from a different site q' , the S matrices can be explicitly constructed by inducing a family of representations from intermediate sites q'' that continuously interpolate between q and q' . A Wyckoff position \mathcal{Q}'' with continuously tunable sites q'' is called *movable* or *non-maximal* when it can continuously preserve $G_{q''}$.

This structure is the mathematical background for the pictures presented in the main text: $S(t, g)$ is the induced representation from the states located at q'' in a path that connects q and q' , and guarantees there exists a gapped, symmetry-preserving path between the different Wannier configurations located at q and q' . We can try to directly find the unitary transformation $U(1, g)$ that transforms $\rho(g)$ into $\tilde{\rho}(g)$. If ρ and $\tilde{\rho}$ are band representations, labelled by k , this implies finding a unitary matrix that is periodic in k and satisfies

$$\rho^{\mathbf{k}}(g) = U_{g\mathbf{k}}^\dagger(1, g) \tilde{\rho}^{\mathbf{k}}(g) U_{\mathbf{k}}(1, g) \quad (\text{C8})$$

for all g and k . While we have argued that all *representations* along a movable path are equivalent, the Wannier states $|\mathbf{R}; q\rangle$ and $|\mathbf{R}; q'\rangle$ are generally different. Additionally, the Hamiltonian itself is not generally left invariant by these transformations, and the path is implemented by varying the Hamiltonian parameters. However, in some cases two different points along the path may simply correspond to a *basis transformation*. In these cases $U_{\mathbf{k}}$ leaves the Hamiltonian invariant. This is relevant for the DMQI example, where the mirror operators anticommute, and the Wannier states can be either at the $2e$ or the $2g$ depending on which M_x or M_y we choose to act diagonally. Thus, whether we draw the Wannier functions in $2e$ or $2g$ is a choice of basis (at least when periodic boundary conditions are chosen).

Appendix D: Bulk band representation of the DMQI model

In this work we claim that the existence of the adiabatic path $S(t, g)$ can be affected by the presence of a boundary. That is, a boundary can disconnect phases that are topologically equivalent on a torus. This is depicted in the main text by showing how the adiabatic path between different Wyckoff positions is obstructed in the presence of a boundary. But this fact is not surprising: the symmetry group of the system with open boundaries G is different from the symmetry group with periodic boundaries $G^{(T)}$, and consequently different obstructions may arise. Although counter intuitive, such obstructions emerge from connected band representations becoming disconnected in a nontrivial fashion.

For the reasons discussed in this Appendix, a boundary obstructed phase cannot be captured by any bulk quantity that

²¹ The notation \uparrow indicates the induced representation

preserves $G^{(T)}$. However, we have discussed at great length in the main text that it can be diagnosed if a property of interest (effectively) reduces $G^{(T)}$ to a subgroup. We have used two methods to accomplish this: either by opening the boundaries (Sec. II B), or calculating the Wannier spectrum (Sec. II C). Other approaches, such as calculating the entanglement spectrum may be found in Ref.[18].

Now we show explicitly that with periodic boundaries there are no distinct topological phases in the DMQI model. The two filled bands are described by a band representation ρ^k which may be induced from any of the four continuously movable Wyckoff positions $2e$, $2f$, $2g$, and $2h$ of multiplicity two, displaced from the maximal Wyckoff positions by a distance δ . The site symmetry group at these Wyckoff positions is C_2^π generated by $\bar{1}$ and a remaining mirror symmetry M . In the presence of translation symmetry the occupied states in each unit cell transform under a two dimensional representation of \bar{E} . In the case of $2e$, these states are explicitly $|R; (\pm\delta, 0)\rangle$.

We now prove that all Wannier configurations in the DMQI are topologically equivalent. Since the maximal Wyckoff positions are reached for $\delta = 0$ or $\delta = 1/2$, we need only to show that band representations induced from all four two-dimensional Wyckoff positions are unitarily equivalent. First, we immediately see that, because of the π flux, $\rho^k(\bar{1}) = -1$ for all Wyckoff positions. We are left to relate $\rho^k(M_x)$ and $\rho^k(M_y)$. Let us first compare $2e$ and $2g$. Inducing the BR from $2e$, we find $\rho_{\bar{E},2e}^k(M_x) = \sigma_1$ and $\rho_{\bar{E},2e}^k(M_y) = \sigma_3$ which are both momentum independent. On the other hand, inducing it from $2g$ we find $\rho_{\bar{E},2g}^k(M_x) = \sigma_3$ and $\rho_{\bar{E},2g}^k(M_y) = \sigma_1$. It

follows that we can relate these two BRs using a momentum-independent transformation $U_k(1, M_x) = \exp\{-i\pi\sigma_2/4\}$ and $U_k(1, M_y) = \exp\{+i\pi\sigma_2/4\}$.

Next we can compare the band representations induced from $2e$ and $2f$ located at two parallel high symmetry lines. Inducing a representation from $2f$ we find that $\rho_{\bar{E},2f}^k(M_x) = \sigma_1$ and $\rho_{\bar{E},2f}^k(M_y) = \exp(ik_y)\sigma_3$. The unitary transformation that relates the $2e$ and $2f$ is

$$U_k(1, M_y) = \frac{1}{2} \begin{pmatrix} 1 + \exp(ik_y) & 1 - \exp(ik_y) \\ 1 - \exp(ik_y) & 1 + \exp(ik_y) \end{pmatrix}. \quad (\text{D1})$$

Interestingly we see that with a unitary transformation that depends (at most) only on k_y , we are able to connect all four maximal Wyckoff positions. This reflects the fact it is sufficient to have periodicity along only one direction in order to lift any boundary obstruction. A similar matrix that was only k_x dependent could also be used.

To emphasize this point we can deduce that there are unitary transformations that act on the DMQI Hamiltonian (1) and change the nested Wannier spectra eigenvalues in either direction. They take the simple diagonal forms

$$\begin{aligned} U_k^x &= \text{diag}(\exp(ik_x), 1, 1, \exp(ik_x)), \\ U_k^y &= \text{diag}(1, \exp(ik_y), 1, \exp(ik_y)), \end{aligned} \quad (\text{D2})$$

where U_k^x changes the nested polarizations $p_{y,x} \rightarrow p_{y,x} + 1/2$, and U_k^y takes $p_{x,y} \rightarrow p_{x,y} + 1/2$.

-
- [1] C. L. Kane and E. J. Mele, Phys. Rev. Lett. **95**, 226801 (2005).
[2] C. L. Kane and E. J. Mele, Phys. Rev. Lett. **95**, 146802 (2005).
[3] B. A. Bernevig, T. L. Hughes, and S.-C. Zhang, Science **314**, 1757 (2006), <http://science.sciencemag.org/content/314/5806/1757.full.pdf>.
[4] X.-L. Qi, T. L. Hughes, and S.-C. Zhang, Phys. Rev. B **78**, 195424 (2008).
[5] J. Moore, Nat. Phys. **5**, 378 (2009).
[6] M. Z. Hasan and C. L. Kane, Rev. Mod. Phys. **82**, 3045 (2010).
[7] X.-L. Qi and S.-C. Zhang, Rev. Mod. Phys. **83**, 1057 (2011).
[8] M. Franz and L. Molenkamp, eds., *Topological Insulators*, Contemporary Concepts of Condensed Matter Science, Vol. 6 (Elsevier, 2013).
[9] A. Kitaev, in *AIP Conference Proceedings*, Vol. 1134 (AIP, 2009) pp. 22–30.
[10] A. P. Schnyder, S. Ryu, A. Furusaki, and A. W. W. Ludwig, in *AIP Conference Proceedings*, Vol. 1134 (AIP, 2009) pp. 10–21.
[11] S. Ryu, A. P. Schnyder, A. Furusaki, and A. W. W. Ludwig, New J. Phys. **12**, 065010 (2010).
[12] P. Dziawa, B. Kowalski, K. Dybko, R. Buczko, A. Szczerbakow, M. Szot, E. Łusakowska, T. Balasubramanian, B. M. Wojek, M. Berntsen, *et al.*, Nature materials **11**, 1023 (2012).
[13] Y. Tanaka, Z. Ren, T. Sato, K. Nakayama, S. Souma, T. Takahashi, K. Segawa, and Y. Ando, Nature Physics **8**, 800 (2012).
[14] W. A. Benalcazar, J. C. Y. Teo, and T. L. Hughes, Phys. Rev. B **89**, 224503 (2014).
[15] W. A. Benalcazar, B. A. Bernevig, and T. L. Hughes, Science **66**, 61 (2017).
[16] W. A. Benalcazar, B. A. Bernevig, and T. L. Hughes, Phys. Rev. B **96**, 245115 (2017).
[17] J. Langbehn, Y. Peng, L. Trifunovic, F. von Oppen, and P. W. Brouwer, Phys. Rev. Lett. **119**, 246401 (2017).
[18] F. Schindler, A. M. Cook, M. G. Vergniory, Z. Wang, S. S. P. Parkin, B. A. Bernevig, and T. Neupert, Science Advances **4**, eaat0346 (2018).
[19] Z. Song, Z. Fang, and C. Fang, Phys. Rev. Lett. **119**, 246402 (2017).
[20] C. Fang and L. Fu, arXiv preprint arXiv:1709.01929 (2017).
[21] E. Khalaf, H. C. Po, A. Vishwanath, and H. Watanabe, Phys. Rev. X **8**, 031070 (2018).
[22] M. Geier, L. Trifunovic, M. Hoskam, and P. W. Brouwer, Phys. Rev. B **97**, 205135 (2018).
[23] E. Khalaf, Phys. Rev. B **97**, 205136 (2018).
[24] L. Trifunovic and P. W. Brouwer, Phys. Rev. X **9**, 011012 (2019).
[25] W. A. Benalcazar, T. Li, and T. L. Hughes, Phys. Rev. B **99**, 245151 (2019).
[26] J. Teo and T. Hughes, Annual Review of Condensed Matter Physics **8**, 211 (2017).
[27] S. Liu, A. Vishwanath, and E. Khalaf, Phys. Rev. X **9**, 031003 (2019).
[28] T. Li, P. Zhu, W. A. Benalcazar, and T. L. Hughes, arxiv:1906.02752 (2019).
[29] B. Bradlyn, L. Elcoro, J. Cano, M. Vergniory, Z. Wang,

- C. Felser, M. Aroyo, and B. A. Bernevig, *Nature* **547**, 298 (2017).
- [30] N. Marzari and D. Vanderbilt, *Phys. Rev. B* **56**, 12847 (1997).
- [31] N. Marzari, A. A. Mostofi, J. R. Yates, I. Souza, and D. Vanderbilt, *Rev. Mod. Phys.* **84**, 1419 (2012).
- [32] R. Yu, X. L. Qi, A. Bernevig, Z. Fang, and X. Dai, *Phys. Rev. B* **84**, 075119 (2011).
- [33] J. Zak, *Physical Review B* **26**, 3010 (1982).
- [34] L. Michel and J. Zak, *EPL (Europhysics Letters)* **50**, 519 (2000).
- [35] M. Vergniory, L. Elcoro, Z. Wang, J. Cano, C. Felser, M. Aroyo, B. A. Bernevig, and B. Bradlyn, *Physical Review E* **96**, 023310 (2017).
- [36] J. Cano, B. Bradlyn, Z. Wang, L. Elcoro, M. Vergniory, C. Felser, M. Aroyo, and B. A. Bernevig, *Physical Review B* **97**, 035139 (2018).
- [37] L. Fidkowski, T. S. Jackson, and I. Klich, *Physical Review Letters* **107**, 1 (2011).
- [38] B. J. Wieder and B. A. Bernevig, arXiv preprint arXiv:1810.02373 (2018).
- [39] H. C. Po, A. Vishwanath, and H. Watanabe, *Nature Communications* **8**, 50 (2017).
- [40] Z. Song, T. Zhang, and C. Fang, *Phys. Rev. X* **8**, 031069 (2018).
- [41] T. L. Hughes, E. Prodan, and B. A. Bernevig, *Phys. Rev. B* **83**, 245132 (2011).
- [42] A. M. Turner, Y. Zhang, R. S. Mong, and A. Vishwanath, *Phys. Rev. B* **85**, 165120 (2012).
- [43] J. Baez, “Torsors made easy,” (2009).
- [44] R. Queiroz, I. C. Fulga, N. Avraham, H. Beidenkopf, and J. Cano, arXiv preprint arXiv:1809.03518 (2018).
- [45] J. C. Y. Teo and C. L. Kane, *Phys. Rev. B* **82**, 115120 (2010).
- [46] L. Fu and C. L. Kane, *Physical Review B* **74**, 195312 (2006).
- [47] J. Cano, B. Bradlyn, Z. Wang, L. Elcoro, M. G. Vergniory, C. Felser, M. I. Aroyo, and B. A. Bernevig, *Physical Review B* **97**, 035139 (2018), arXiv:1709.01935.